

THE ACS VIRGO CLUSTER SURVEY XV. THE FORMATION EFFICIENCIES OF GLOBULAR CLUSTERS IN EARLY-TYPE GALAXIES: THE EFFECTS OF MASS AND ENVIRONMENT¹

ERIC W. PENG^{2,3,4}, ANDRÉS JORDÁN^{5,6,7,8}, PATRICK CÔTÉ², MARIANNE TAKAMIYA⁹, MICHAEL J. WEST^{10,11,9}, JOHN P. BLAKESLEE^{2,12}, CHIN-WEI CHEN^{2,13}, LAURA FERRARESE², SIMONA MEI^{14,15}, JOHN L. TONRY¹⁶, AND ANDREW A. WEST¹⁷

Accepted for publication in the Astrophysical Journal

ABSTRACT

The fraction of stellar mass contained in globular clusters (GCs), also measured by number as the specific frequency, is a fundamental quantity that reflects both a galaxy's early star formation and its entire merging history. We present specific frequencies, luminosities, and mass fractions for the globular cluster systems of 100 early-type galaxies in the ACS Virgo Cluster Survey. This catalog represents the largest homogeneous catalog of GC number and mass fractions across a wide range of galaxy luminosity ($-22 < M_B < -15$). We find that 1) GC mass fractions can be high in both giants and dwarfs, but are universally low in galaxies with intermediate luminosities ($-20 < M_B < -17$). 2) The fraction of red GCs increases with galaxy luminosity, but stays constant or decreases for galaxies brighter than $M_z = -22$. As a result, although specific frequencies for blue and red GCs are both higher in massive galaxies, the behavior of specific frequency across galaxy mass is dominated by the blue GCs. 3) The GC fractions of low-mass galaxies exhibit a dependence on environment, where dwarf galaxies closer to the cluster center have higher GC fractions. Nearly all dwarfs with high GC fractions are within 1 Mpc of the cD galaxy M87, presenting the first strong evidence that GC formation in dwarf galaxies is biased toward dense environments. 4) GC formation in central dwarfs is biased because their stars form earliest and most intensely. Comparisons to early-type dwarf galaxies in the Millennium Simulation show that central dwarfs are likely to have older stellar populations and form more of their stars at higher star formation rates (SFRs) and star formation rate surface densities. In addition, the SFR surface density in simulated dwarfs peaks *before* the total SFR, naturally producing GC populations that are older and more metal-poor than the field stars. 5) Dwarfs within ~ 40 kpc of the giant ellipticals M87 and M49 are red for their luminosities and have few or no GCs, suggesting that they have been tidally stripped and have contributed their GCs to the halos of their giant neighbors. The central dwarfs with high GC mass fractions are thus likely to be the survivors most similar to the protogalaxies that assembled the rich M87 globular cluster system.

Subject headings: galaxies: elliptical and lenticular, cD — galaxies: dwarf — galaxies: halos — galaxies: evolution — galaxies: star clusters — globular clusters: general

1. INTRODUCTION

Globular clusters (GCs) constitute a small fraction of the stellar mass in galaxies, but their ubiquity, relative simplicity, and old ages make them the most prominent representatives of a bygone epoch of galaxy formation. GCs are made of stars that are among the oldest in galaxies, and they can be observed at large distances (e.g., Blakeslee et al. 2003a). These old star clusters are thus unique, both intrinsically and observationally, for understanding the early, intense star-forming episodes that mark galaxy formation.

In the local universe, we see massive star clusters forming wherever there are high star formation rate surface densities (Larsen & Richtler 2000), providing a connection that suggests the properties of star cluster populations—age, metallicity, mass—should scale quite closely with field stars formed in the same events. The properties of globular cluster systems do in fact correlate strongly with the properties of the field stars of their host galaxies. The mean metallicities of GC systems have long been known to scale with the metallicity of their

¹⁶ Institute for Astronomy, University of Hawai'i, 2680 Woodlawn Drive, Honolulu, HI 96822, USA

¹⁷ Department of Astronomy, University of California, 601 Campbell Hall, Berkeley, CA 94720

¹ Based on observations with the NASA/ESA *Hubble Space Telescope* obtained at the Space Telescope Science Institute, which is operated by the Association of Universities for Research in Astronomy, Inc., under NASA contract NAS 5-26555.

² Herzberg Institute of Astrophysics, National Research Council of Canada, 5071 West Saanich Road, Victoria, BC V9E 2E7, Canada; Eric.Peng@nrc-cnrc.gc.ca

³ Space Telescope Science Institute, 3700 San Martin Drive, Baltimore, MD, 21218, USA

⁴ Department of Astronomy, Peking University, Beijing 100871, China

⁵ Harvard-Smithsonian Center for Astrophysics, 60 Garden St., Cambridge, MA 02138

⁶ Clay Fellow

⁷ European Southern Observatory, Karl-Schwarzschild-Str. 2, 85748 Garching bei München, Germany

⁸ Departamento de Astronomía y Astrofísica, Pontificia Universidad Católica de Chile, Casilla 306, Santiago 22, Chile

⁹ Department of Physics & Astronomy, University of Hawai'i, 200 W. Kawili Street, Hilo, HI 96720, USA

¹⁰ European Southern Observatory, Alonso de Cordova 3107, Vitacura, Santiago, Chile

¹¹ Gemini Observatory, Casilla 603, La Serena, Chile

¹² Department of Physics and Astronomy, Washington State University, Pullman, WA 99164-2814

¹³ Institute for Astronomy, National Central University Taiwan, Chung-Li 32054, Taiwan

¹⁴ University of Paris 7 Denis Diderot, 75205 Paris Cedex 13, France

¹⁵ GEPI, Observatoire de Paris, Section de Meudon, 5 Place J. Janssen, 92195 Meudon Cedex, France

host (van den Bergh 1975; Brodie & Huchra 1991), and the mean metallicities of both the metal-rich and metal-poor subpopulations also correlate with the luminosity and mass of the host galaxy (Larsen et al. 2001; Peng et al. 2006a and references therein). However, if GC systems directly followed the underlying field light in every way, they might be less interesting. For instance, although the metallicities of GC systems may track those of galaxies, they are consistently offset to lower values by ~ 0.5 – 0.8 dex in $[\text{Fe}/\text{H}]$ (e.g., Jordán et al. 2004a, Lotz et al. 2004). Most conspicuously, even the most massive and metal-rich galaxies have GC systems dominated by metal-poor star clusters ($[\text{Fe}/\text{H}] \lesssim -1$). This suggests a disconnect between the formation of “halo” stellar populations and the bulk of the galaxy.

One of the most studied aspects of this GC–galaxy duality concerns the specific frequency of globular clusters, or the number of GCs per unit stellar luminosity. Specific frequency, S_N , was introduced by Harris & van den Bergh (1981) and is defined as the number of GCs normalized to a galaxy luminosity of $M_V = -15$. The purpose of studying S_N across galaxies of different masses, morphologies, and environments is, in the words of that initial paper, “to investigate whether there is in fact a ‘universal’ and uniform capability for globular cluster formation”. This simple quantity, and similar ones related to it, turn out to be extremely interesting galaxy diagnostics. It appears true that for galaxies above a certain mass there is a nearly universal capability to form globular clusters, but this process is not uniform across all galaxies, at least as seen in comparison to the field stars. Specific frequencies of spiral galaxies like the Milky Way are generally 0.5–1 (Goudfrooij et al. 2003; Rhode & Zepf 2004; Chandar, Whitmore & Lee 2004), although they have a mean of ~ 4 when normalized only to bulge luminosity (Côté et al. 2000). The specific frequencies of massive ellipticals are 2–6, and those of some cD galaxies such as M87 (N4486) can be well in excess of 10. These trends are apparent even when the number of GCs is normalized to stellar mass as opposed to stellar luminosity (Rhode, Zepf & Santos 2005). Dwarf elliptical galaxies (dEs), whose GC systems are predominantly metal-poor, can also have high S_N similar to those of giant ellipticals (Durrell et al. 1996; Miller et al. 1998; Lotz et al. 2004; Miller & Lotz 2007; Puzia & Sharina 2007), as can some dwarf irregulars (Seth et al. 2004), suggesting the possibility that the halos of large galaxies were formed mainly through the accretion of dwarf-like objects (Searle & Zinn 1978; Côté, Marzke & West 1998; Côté et al. 2000).

A central question in the study of GC systems is: How do we understand different GC fractions in the context of galaxy assembly? The formation of globular cluster systems has been particularly tied to the formation of massive elliptical galaxies, in which GCs are often present in large numbers and where GCs are most easily observed. The mergers and accretion events expected during the hierarchical assembly of these galaxies must also be able to form their GC systems. Observations and simulations of elliptical galaxy formation are creating a picture in which the stars form early and quickly (e.g., Kodama et al. 1998), mimicking the traditional “monolithic collapse” scenario, but where the assembly of these stars into a single galaxy continues until late times through largely dissipationless mergers (De Lucia et al. 2006; De Lucia

& Blaizot 2007), and star formation at late times is suppressed by energy feedback (Springel et al. 2005; Croton et al. 2006).

Intertwined with the issue of galaxy formation is that of the formation efficiency of the GCs themselves: Why do globular clusters form with different efficiencies with respect to their light in different galaxies? Blakeslee, Tonry & Metzger (1997) and Blakeslee (1999) studied the GC systems of brightest cluster galaxies (BCGs) in Abell galaxy clusters and found that the number of GCs scaled with the velocity dispersion of the galaxy cluster rather than with the luminosity of the BCGs, suggesting that GC formation is closely linked to the total mass of the system, i.e., $S_N \propto \mathcal{M}/L$. In a similar vein, McLaughlin (1999a) examined the high S_N in M87 and found that the large number of GCs it possessed was not anomalous when normalized to the total baryonic mass (including the hot X-ray gas) rather than just to the stellar mass. McLaughlin (1999a) defined a “universal” GC formation efficiency of $\hat{\epsilon} = 0.26\%$, where $\hat{\epsilon}$ is the fraction of the baryonic mass that ends up in globular clusters. Kravtsov & Gnedin (2005) studied the formation of the GC system in a high resolution hydrodynamic simulation and also found that the mass in GCs was directly proportional to the total halo mass of the galaxy. If total mass drives GC formation, then it is the variation in converting baryons into field stars that drives trends in specific frequency.

The connection between GCs and galactic mass (baryonic or total) makes it tempting to try to explain them using simulations of dark matter and galaxy assembly. Beasley et al. (2002) simulated the color distributions of GCs using semi-analytic models of galaxy formation, while the aforementioned simulations of Kravtsov & Gnedin (2005) formed a Milky Way mass galaxy in detail. Moore et al. (2006) identified metal-poor GCs with early collapsing dark matter peaks in cosmological N-body simulations. An empirical connection between the total mass of a system and the mass contained in its globular clusters does not, however, explain why the star formation histories of the GCs and the field should be different.

One clue is that in the local Universe, high mass fractions in massive star clusters occur in regions of high star formation surface density (Larsen & Richtler 2000). Thus, one explanation for high- S_N galaxies might be that they formed more of their stars in high efficiency events. Given that the star formation rate (SFR) in galaxies was most intense at very early times ($z \gtrsim 2$), variations in S_N could result from different times of formation, especially when coupled with a sharp star formation cutoff at reionization (Santos 2003). In this scenario, with S_N a function of formation time, GC formation is biased towards the earliest collapsing halos which can create a large fraction of their stars at high efficiency before reionization. Low mass halos in dense environments collapse earlier (Gao, Springel & White 2005; Diemand, Madau & Moore 2005), and these are also the ones most susceptible to heating through photoionization and feedback. One expectation of this scenario is that S_N will be “biased” towards dense environments (West 1993), especially in low mass galaxies. The simulations of Moore et al. (2006) suggested that GCs and satellites would be more highly clustered in dense regions for higher redshifts of reion-

ization, and the same idea can be applied to S_N at fixed reionization redshift.

Previous observational studies have shown some evidence of an environmental dependence for S_N . West (1993) showed that the mean S_N of elliptical galaxies correlates with the local galaxy density. Blakeslee (1997, 1999) found that S_N in brightest cluster galaxies (BCGs) scaled with properties that reflect cluster density (cluster velocity dispersion, X-ray temperature, and X-ray luminosity), and that cluster galaxies closer to their cluster’s X-ray center have higher S_N . West et al. (1995) also found a correlation between the S_N of BCGs and the X-ray luminosity of the cluster, interpreting it as evidence for a population of intergalactic globular clusters. On the other hand, Lotz et al. (2004) and Miller & Lotz (2007) did not find an obvious correlation between S_N and clustercentric radius for dEs in the Virgo and Fornax clusters, although the number of GCs in their galaxies were small and S_N errors were quite large. Also, Spitler et al. (2007) recently found that the relatively isolated elliptical NGC 821 has an S_N comparable to cluster galaxies of like luminosities.

The specific frequencies (or formation efficiencies) of globular cluster systems is clearly a fundamental property of galaxies. However, accurately measuring S_N is traditionally fraught with uncertainty despite the fact that at its most basic level it requires only simple counting of GCs. In practice, observations need to be deep enough to observe past the mean of the GC luminosity function, and GC selection needs to be efficient enough so that contaminants do not overwhelm the GCs in lower mass galaxies. The total magnitude and distance of the galaxy also needs to be known to establish its luminosity (or mass). Studies of larger galaxies also benefit from wide-field coverage so that enough of the GC system is sampled to minimize extrapolation errors. It is because of these limitations that homogeneous surveys of S_N across a wide range of galaxy mass are difficult to conduct. To put together a complete picture of globular cluster system and galaxy formation, it is important to study galaxies at all masses in the same way—at low masses we study the survivors of hierarchical assembly, and at high masses we study its final products.

With this in mind, we have undertaken a careful study of the formation efficiencies for the GC systems of 100 early-type galaxies in the ACS Virgo Cluster Survey (ACSVCS; Côté et al. 2004). The deep, high-resolution, relatively wide-field imaging provides the most complete census to date of GCs in early-type galaxies over a large range in galaxy luminosity ($-22 < M_B < -15$). In this paper, we present the specific frequencies and other related quantities of the ACSVCS galaxies and quantify their trends as a function of host galaxy properties.

2. OBSERVATIONS AND DATA

The ACS Virgo Cluster Survey (ACSVCS) is a large program to image 100 early-type galaxies in the Virgo Cluster with the HST Advanced Camera for Surveys (ACS; Ford et al. 1998). The survey is described in detail in Paper I (Côté et al. 2004), and the data reduction techniques are outlined in Jordán et al. 2004b (Paper II), but we briefly summarize them here. We obtained images in the F475W (g) and F850LP (z) filters of galaxies selected to be early-type and with con-

firmed cluster membership in the Virgo Cluster Catalog (VCC) of Binggeli, Sandage, & Tammann (1985). Our sample excludes the Southern Extension, has $B_T < 16$, and the galaxies are morphologically classified as E, S0, dE, dE,N, dS0, or dS0,N. This early-type galaxy sample is magnitude limited for the brightest 26 galaxies ($B_T < 12.15$ or $M_B < -19.10$), and contains a representative sample of galaxies for $M_B < -15.11$. The color distributions of the GC systems were presented in Peng et al. (2006a; Paper IX), and their size distributions in Jordán et al. (2005; Paper X). We have measured distances for 84 galaxies from the method of surface brightness fluctuations (Mei et al. 2005a, 2005b, 2007; Papers IV, V, and XIII). For galaxies where an SBF distance could not be measured, we adopt a distance to the Virgo Cluster of $D = 16.5$ Mpc with a distance modulus of 31.09 ± 0.03 mag from Tonry et al. (2001), corrected by the final results of the Key Project distances (Freedman et al. 2001; see also discussion in Mei et al. 2005b). The surface brightness profiles, total magnitudes, and colors of the sample galaxies in g and z were described in Ferrarese et al. (2006a; Paper VI), and the properties of the GC luminosity functions for 89 of our sample galaxies were presented in Jordán et al. (2007a, 2007b, Paper XII). The galaxy nuclear properties were presented in Côté et al. (2006; Paper VIII) and their connection to supermassive black holes in Ferrarese et al. (2006b). These data have also been analyzed for ultra-compact dwarf galaxies (Hasegan et al. 2005; Paper VII), diffuse star clusters (Peng et al. 2006b; Paper XI), the connection between GCs and low mass X-ray binaries (Jordán et al. 2004c, Sivakoff et al. 2007), and color-magnitude relations in GC systems (Mieske et al. 2006; Paper XIV). Together, these data create the best opportunity to date to study the formation efficiencies of GC systems in early-type galaxies, and this paper will refer often to the quantities measured in the preceding papers.

2.1. Data Reduction and Control Fields

Each galaxy was imaged with the Wide Field Channel (WFC) of the ACS. We reduced the ACS/WFC images using a dedicated pipeline described in Jordán et al. (2004b, Paper II; see also Blakeslee et al. 2003b). We produced the science images by combining and cleaning them of cosmic rays using the Pyraf routine *multidrizzle* (Koekemoer et al. 2002). We then subtracted a model of the galaxy light and used the source detection program SExtractor (Bertin & Arnouts 1996) to detect and mask sources and remove residual background. Our final object detection includes estimates of both the image noise and noise due to surface brightness fluctuations—ignoring the latter results in many false detections in the bright central regions of the galaxy—and objects are only included in the final catalog if they are detected in both filters. After rejecting very bright or elongated objects to eliminate obvious foreground stars and background galaxies, and passing our catalog through a generous color cut, we use the program KINGPHOT (Jordán et al. 2005) to measure magnitudes and King model parameters. KINGPHOT fits King (1966) model surface brightness profiles convolved with the filter- and spatially-dependent point spread function (PSF). Magnitudes and colors are corrected for foreground extinction using the reddening maps of Schlegel, Finkbeiner, &

Davis (1998) and extinction ratios for a G2 star (Paper II; Sirianni et al. 2005). For the purposes of this paper, whenever we refer to g and z , we mean the HST/ACS magnitudes g_{475} and z_{850} . Magnitudes in the Sloan Digital Sky Survey (SDSS) system will be designated explicitly, e.g., as in g_{sdss} . The low redshifts of the galaxies being studied (-575 to 2284 km s^{-1}) means that K -corrections are negligible and thus we do not K -correct any of the magnitudes presented in this paper.

In any study of extragalactic star clusters, it is important to quantify and correct for background contamination. To that end, we have also reduced 16 blank, high-latitude control fields taken from the ACS Pure Parallel Program (GO-9488, PI: Ratnatunga; and GO-9575, PI: Sparks). For each galaxy, we have “customized” the control sample to mimic the spatially varying detection efficiency that is a function of the surface brightness of the unresolved galaxy light. Details of this procedure are given in Peng et al. (2006a,b; Papers IX and XI).

We select probable globular clusters using their sizes and magnitudes. We can assign a probability that any object is a GC based on position in the r_h - z diagram and the locus of contaminants in the same plane. Objects with probabilities greater than 0.5 are included in our GC sample, although the exact choice of the cutoff value does not significantly affect our results. We describe the details of this selection in Peng et al. (2006a, Paper IX) and Jordán et al. (2008, in preparation).

2.2. WFPC2 Parallel Fields

In addition to ACS/WFC imaging of our target galaxies, we have also acquired parallel imaging of 100 “blank” fields using the Wide Field Planetary Camera 2 (WFPC2) in the F606W (wide V) and F814W (I) filters. The separation between ACS and WFPC2 in the HST focal plane is approximately $5/8$, which is 29 kpc at the mean distance to the Virgo cluster (16.5 Mpc). For most of the ACSVCS galaxies, this distance puts the WFPC2 field well outside of the target galaxy, and thus one motivation for taking them is to search for intergalactic GCs (e.g., West et al. 1995, Jordán et al. 2003, Williams et al. 2007). In this paper, we use the WFPC2 parallel images instead to constrain the total number of GCs in the larger, more luminous galaxies, where the GC system is still detectable 29 kpc from the center. The WFPC2 images were reduced using a modified form of the PyRAF pipeline written by Alasdair Allan¹⁸. We implemented the cosmic ray cleaning algorithm LACOSMIC (van Dokkum 2001) and a geometric distortion correction (Bagget et al. 2002) in the PyRAF pipeline. Sources were selected from a SExtractor catalog having magnitudes and colors of GCs. The sizes and magnitudes of GC candidates were also measured with KINGPHOT. To account for sample contamination, we selected 10 blank WFPC2 fields from the HST archive of similar depth and observed with the same filters as our WFPC2 data. We analysed them in the same manner as our data, using WFPC2 point spread functions provided by P. B. Stetson. We find that there are on average 5.8 ± 2.5 contaminant sources per WFPC2 field.

3. CALCULATING SPECIFIC FREQUENCIES, LUMINOSITIES, AND MASSES

3.1. Total Numbers of GCs

The determination of specific frequency requires knowledge of the total numbers of GCs, the total apparent magnitude of the galaxy (traditionally in the V band), and the distance. For the distances, we use the SBF-determined distances presented in Mei et al. (2007; Paper XIII), using their polynomial calibration. The measurement of the total number of GCs is in principle a simple task of counting, but is not quite so straightforward in practice. Our images are deep enough that we generally detect the brightest $\sim 90\%$ of the GC luminosity function (GCLF), limiting the uncertainties from extrapolations in luminosity. Nevertheless, a full count of the GCs within the ACS field of view involves knowing our level of completeness, which is a function of the GC magnitude, size, and the local background flux. We also need to know the form of the GCLF so that we can estimate the number of GCs missed.

Fortunately, both the level of completeness and the GCLF can be determined for our data. We empirically derived the completeness of our data as a function of magnitude, background flux, and GC size, using simulations of nearly 5 million GCs placed in actual ACSVCS images for galaxies of different surface brightnesses. Using these data, we can nonparametrically estimate the expected detection probability of any GC in the survey. In addition, Jordán et al. (2007; Paper XII) was able to determine the form of the GCLF for 89 galaxies in the survey. For galaxies where we were unable to measure the form of the GCLF we assume the mean to be the same as that of the cD galaxy VCC 1316, and a Gaussian distribution with sigma derived from Equation 2 in Jordán et al. (2006). In this paper, we will use the Gaussian parameterization of the GCLF.

Most of our galaxies are small enough that the ACS/WFC field of view is sufficient to encompass all of the galaxy’s GC system. In these cases, we determine the total number of GCs by counting GC candidates within our imaged field, correcting for incompleteness using the known mean and sigma of the GCLF. Calculating the completeness correction, however, is not straightforward because the surface brightness of the galaxy varies spatially. If, for instance, there were strong radial gradients in the GCLF or size distribution, we could be over- or under-correcting for unseen GCs. Our previous work on these galaxies (Jordán et al. 2005, 2007) shows that this is not likely to be the case. We use bright GCs ($z < 22.5$)—those that are bright enough as to be complete over the entire range of galaxy surface brightness and GC sizes—to sample the “true” distribution of background surface brightnesses and GC sizes. We then make the assumption that the fainter GCs sample the same distributions to derive a mean completeness correction for the entire population.

In the more luminous galaxies, the ACS/WFC field of view is insufficient to image the entire GC system. To correct for this, we determine the radial spatial density profile of the GC system, fit a Sérsic profile, and integrate over all radii to estimate the total number of GCs. For the largest galaxies, we supplemented the density profiles at larger radii with data from three sources: 1)

¹⁸ http://www.astro.ex.ac.uk/people/aa/pages/computing/pyraf_pipeline.html

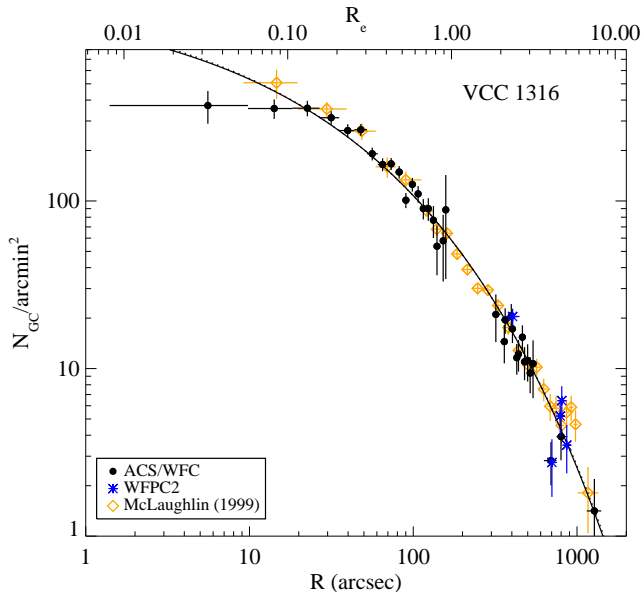


FIG. 1.— Surface density of globular clusters in VCC 1316 (M87/N4486) as a function of projected galactocentric radius. We use data from three sources to fit the spatial density profile: ACS pointings of the central field and companion fields (black dots), WFPC2 parallel pointings in adjacent blank fields (blue asterisks), and ground-based data from McLaughlin (1999a) (orange diamonds). All data are in good agreement and are well fit by a Sérsic profile (black line). We integrate the Sérsic profile to obtain the total number of GCs.

ACSVCS imaging of companion galaxies whose GC systems are dominated by the halo population of the neighboring giant, 2) Our WFPC2 parallel imaging of nearby halo fields (Takamiya et al., in prep), and 3) Ground-based data from the literature. In cases where there is no wide-field ground-based data, our additional pencil-beam HST/WFC and WFPC2 observations still do a comparably good job because the spatial resolution of HST minimizes the noise from background contamination. We use the same method described above for completeness correction, except we do so in bins of galactocentric radius instead of for the whole field of view.

Errors for N_{GC} were determined using a Monte Carlo technique where we introduced the appropriate random Poisson noise to our density profiles, then fit and integrated the Sérsic (1968) profile. After doing this 1000 times, we used the distribution of estimated N_{GC} to determine the intervals that contained the closest 68% of the measurements to the mean. In Figure 1, we show the combined radial profile data for VCC 1316 (M87/N4486, hereafter M87), which includes the central ACS pointing, four ACS pointings targeted at nearby companions, WFPC2 pointings, and the ground-based data of McLaughlin (1999a). All are in good agreement and are well fit by a Sérsic profile, except perhaps in the very central regions which are difficult to measure (especially from the ground) and do not contribute large numbers of GCs. The spatial density profiles of the GC systems of ACSVCS galaxies will be presented in Peng et al. (in prep), which will contain a more detailed description of the techniques. Below, we outline our use of supplementary data in the larger galaxies.

VCC 1226 (M49/N4472, hereafter M49). For the most luminous galaxy in the Virgo cluster, we used the GC

counts in the fields of the neighboring compact galaxies VCC 1192 and 1199, excluding a region of $4 R_e$ around the galaxies themselves, where R_e is the effective radius. We also used four WFPC2 parallel fields in the halo, and the ground-based density profiles of McLaughlin (1999a) and Rhode & Zepf (2001). All these data are in excellent agreement.

VCC 1316 (M87/N4486). Four ACSVCS galaxies are near enough to this cluster cD that the GCs observed in their images are dominated by those of the giant: VCC 1327 (NGC 4486A), VCC 1297 (NGC 4486B), VCC 1279 and VCC 1250. VCC 1250 also appears to have ongoing star formation. As described above for M49, we masked a region of $4 R_e$ around these nearby neighbors and used the remaining GCs to constrain the density profile of the larger galaxy. In addition, we used five WFPC2 parallel fields, and the ground-based density profiles from McLaughlin (1999a) (see Figure 1).

VCC 881 (N4406). We supplemented the profile with two WFPC2 fields and the ground-based density profile of Rhode & Zepf (2004).

VCC 763 (N4374). We supplemented the profile with two WFPC2 fields and the ground-based density profile of Gómez & Richtler (2004).

VCC 798, 731, 1535, 1903, 1632, 1231, 2095, 1154, 1062, 1030, and 1664. For these galaxies, we extended the measured density profile using between 1 and 3 WFPC2 fields per galaxy, which were at galactocentric radii between $5'$ and $17'$.

When we compare the total number of GCs derived using the integrated GC radial density profiles against the total number counted within the ACS/WFC field of view, the numbers converge for galaxies with $M_B > -18$. Because integrated radial density profiles are more uncertain and not necessary in low luminosity galaxies, we have adopted $M_B = -18$ as a cutoff; for galaxies brighter than this, we use the Sérsic-integrated GC number counts, and for galaxies fainter than this, we use the corrected number of GCs directly counted within the ACS/WFC image.

VCC 1938 has a close companion dE, VCC 1941, whose GC system complicates an accurate count of the larger galaxy's GC system. We mask a $R = 70''$ region around VCC 1941, and count only GCs in the ACS/WFC field of view, so our count of the VCC 1938 GC system is likely to be a lower limit.

All GC counts are corrected for foreground and background contamination using control fields (except in the eight cases described below). In many other studies, the background is taken from an annulus around the target galaxy. The advantages of using separate control fields are: 1) We can sample a much larger area of sky to determine the mean surface density of contaminants, thus greatly reducing the Poisson errors introduced in contaminant subtraction, 2) We can use the full field of view for the target galaxy to measure as much of the GC system as we can, 3) We can still study systems where the GC system fills the entire field of view, 4) We can naturally incorporate spatially varying completeness as a function of position within the galaxy. The only potential disadvantage is the addition of cosmic variance into the error.

The advantage in using multiple control fields over a local background approach is most clear for the dwarf galaxies that have few GCs, where we need to minimize

the error in the mean expected background. We determine the error in the background by measuring the number of GC-like objects selected in each of the 16 custom control fields, and taking the standard deviation of these counts. This number combines both Poisson errors and cosmic variance, and takes into account the varying selection and completeness from galaxy-to-galaxy. We find that the contribution of cosmic variance to the errors is on the order of the Poisson noise or less, and that the use of control fields is superior to the use of a local background.

For eight galaxies—VCC 1327, 1297, 1279, 1250, 1185, 1192, 1199, 1178—control fields are insufficient, and we measure the total number of GCs by counting candidates in a $R = 70''$ aperture and subtracting a local background. The first five are nearby neighbors to the giant elliptical M87 and so some (and sometimes all) GCs detected in their vicinity belong to the halos of the giants. The next three are neighbors of M49. The size of this aperture was chosen to fit the ACS/WFC field of view, and extends 11, 30, 4, 4, 10, 20, 11, and 5 R_e in radius for these galaxies, respectively. These numbers are, in principle, lower limits to the total numbers of GCs in each system.

In total, we present a homogeneous catalog of GC number counts for 100 ACSVCS galaxies. We have taken great care in this paper to produce our best estimate for the total number of GCs in the ACSVCS galaxies. Peng et al. (2006a) listed numbers of GCs used in their analysis of color distributions, but *we emphasize that those numbers were not corrected for field of view or completeness* and are best used only to evaluate the signal-to-noise ratio of the color distributions. Forbes (2005) and Miller & Lotz (2007) both derive S_N values from Peng et al. (2006a) (the Forbes (2005) paper uses them exclusively), and so the appropriate warnings apply.

3.2. Total Luminosities and Masses of GCs

Another quantity of interest is the total luminosity (or stellar mass) in GCs. We take a straightforward empirical approach to measuring the total luminosity. For each galaxy, we add up the z -band luminosity in observed GCs down to 1 mag fainter than the mean of the GCLF, with adjustments for contaminants and completeness. For galaxies with $M_B < -18$, we apply an aperture correction to the total luminosity in GCs, which is the ratio of the total number of GCs determined from the integrated radial profile to the total number observed in the ACS/WFC image. At this depth, we are directly counting 84% of the GCs in a Gaussian GCLF, but are sampling 99% of the luminosity in GCs. Thus, completeness corrections are small, and it has been advocated (e.g. Harris 1991) that the luminosity in GCs is a more robust quantity than the number of GCs. To obtain the total mass in GCs, we assume that each GC is a 13 Gyr simple stellar population (SSP) (Chaboyer et al. 1996) and use its $(g-z)$ color in conjunction with the Bruzual & Charlot (2003; BC03) models with a Chabrier (2003) initial mass function (IMF) to obtain a mass-to-light ratio in the z bandpass. The range of \mathcal{M}/L_z variation with $[\text{Fe}/\text{H}]$ for globular clusters is no more than $\pm 20\%$.

3.3. Galaxy Magnitudes:

A Consistent Catalog of M_V And M_z

Globular cluster formation efficiencies can be measured against the total luminosity or mass of a galaxy. Specific frequency is typically calculated using the absolute V magnitude. The Virgo Cluster Catalog lists M_B for all of our sample galaxies, but these magnitudes were not derived from CCD photometry. We do not have V imaging for our galaxies, so we predict V using optical colors measured from SDSS imaging. We use $(ugriz)_{sdss}$ photometry measured directly from images in the Sloan Digital Sky Survey Data Release 5 (Adelman-McCarthy et al. 2007). In many cases the large sizes of the galaxies compared to the size of the SDSS CCDs required careful stitching of neighboring runs and camera columns to produce flat images with matching sky (West et al. 2007). Using these specially prepared images, we measured total magnitudes in the five SDSS bands for all the ACSVCS galaxies using a growth curve analysis. Details of this analysis and the full catalog of magnitudes and colors will appear in Chen et al., in prep.

For the purposes of this paper, we only use the SDSS photometry for two objectives, deriving a V magnitude, and supplementing the total z magnitudes given in Paper VI derived from ACS imaging. For determining each galaxy's V magnitude, we fit SSPs from BC03 to the four optical colors— $(u-g)_{sdss}$, $(g-r)_{sdss}$, $(r-i)_{sdss}$, $(i-z)_{sdss}$ —and use the $g_{sdss} - V$ color of the best fit model. Across the entire sample, the $g_{sdss} - V$ color ranges from 0.18 to 0.48 with a mean of 0.37. In practice, this approach is extremely robust because $g_{sdss} - V$ is almost entirely a function of $(g-r)_{sdss}$. We subtract this color from the measured g_{sdss} magnitude to obtain V . The mean relationship between V and $(g-r)_{sdss}$ matches the empirical relation of Blanton & Roweis (2007), except that our magnitudes are fainter in the mean by 0.03 mag.

Because redder wavelengths are a better tracer of stellar mass than the traditionally used B and V , we will often use the total integrated z luminosities of galaxies in this paper. For most of these galaxies, we use the z magnitudes measured from the ACS images as presented in Paper VI. However, for the brightest 10 galaxies, the ACS field of view was substantially smaller than the extent of the galaxy, and we prefer to use the wide-field SDSS photometry (after introducing a small (< 0.04 mag) color-dependent correction between the SDSS to the ACS photometric systems). We also use the SDSS photometry for VCC 1030, 575, and 1512, which have suspect integrated magnitudes from their ACS surface brightness profiles (see notes on these galaxies in Paper VI). Otherwise, the two independent measures of the total luminosity are in good agreement. We choose to use the ACS magnitudes for the remaining 87 galaxies because they have higher signal-to-noise than the SDSS photometry, which were taken from the ground with much higher sky backgrounds and shorter exposures.

3.4. Stellar Mass

Stellar mass is a better basis for comparison when studying galaxies of different morphological types and star formation histories. The V band light in star-forming galaxies is affected significantly by young stars and is not the best tracer of the total mass. Using the $(g-z)$ colors from Paper VI, $J - K_s$ colors from the Two Micron All Sky Survey (2MASS; Skrutskie et al. 2006), and the model SSPs from BC03 with a Chabrier (2003)

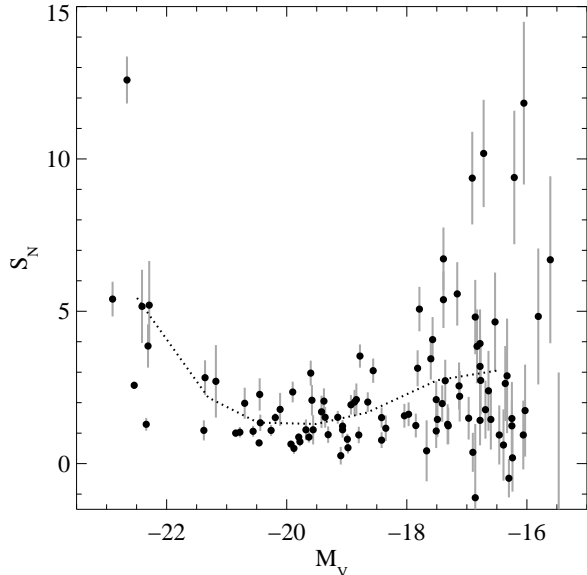


FIG. 2.— S_N versus galaxy M_V for 100 ACSVCS galaxies. M87, the giant elliptical with $S_N \sim 13$ is a well-known outlier. Luminous early-type galaxies have higher S_N than intermediate-luminosity early-type galaxies by a factor ~ 2 -3. Galaxies with intermediate luminosities ($-20.5 < M_V < -18$) generally have $S_N \sim 1.5$. Early-type dwarf galaxies have a large spread in S_N , with some having zero GCs, and others having among the highest measured S_N in our sample. The dotted line shows the mean trend (including M87) whose values are listed in Table 3.

initial mass function, we obtain mean mass-to-light ratios in the z bandpass (\mathcal{M}/L_z) from which we can derive a total stellar masses. In the near-infrared, we measure the J and K_s galaxy magnitudes in images taken by 2MASS, and supplement them with those in the 2MASS Extended Source Catalog (XSC) and Large Galaxy Atlas (Jarrett et al. 2003). For 9 galaxies with unreliable K_s photometry from 2MASS (those not included in the XSC), we use only the $(g-z)$ color assuming a 10 Gyr SSP to determine \mathcal{M}/L_z . We assume a younger age than for GCs because dEs are measured to have younger ages than GCs or massive ellipticals (Geha et al. 2003). Although \mathcal{M}/L is related to both age and metallicity, it is easier to determine \mathcal{M}/L than age or metallicity individually. Most of the sample have \mathcal{M}/L_z consistent with old stellar populations (age > 5 Gyr), though a few galaxies are dE/dI transition objects and have noticeably younger mean ages and correspondingly lower \mathcal{M}/L_z (the most extreme example being VCC 1499). For one of these galaxies, VCC 1030, we derive a low mean age, high metallicity, and a correspondingly low \mathcal{M}/L_z . While this galaxy may be interacting, the colors may also be suspect due to a large-scale central dust disk. Until we get more data, we consider \mathcal{M}/L for this galaxy uncertain.

Fortunately, the z bandpass is less sensitive to recent star formation than bluer bandpasses, and the range of \mathcal{M}/L_z is only 0.4 to 2.1, a dynamic range which is a factor of ~ 3 smaller than that for \mathcal{M}/L_B . The error in \mathcal{M}/L_z is dominated by the quality of the infrared photometry. We estimate errors in \mathcal{M}/L_z with a Monte Carlo procedure where the $J - K_s$ color is perturbed by a random amount drawn from a Gaussian distribution with sigma equal to the claimed photometric error. The

TABLE 3
SPECIFIC FREQUENCY IN
BINS OF M_V

M_V range	$\langle M_V \rangle$	S_N
$(-24, -22)^1$	-22.5	4.0
$(-24, -22)$	-22.5	5.4
$(-22, -21)$	-21.3	2.2
$(-21, -20)$	-20.5	1.3
$(-20, -19)$	-19.5	1.3
$(-19, -18)$	-18.7	1.7
$(-18, -17)$	-17.5	2.7
$(-17, -15)$	-16.4	3.1

¹Not including VCC 1316 (M87)

\mathcal{M}/L_z is then recalculated in this fashion 1000 times and the error is the half width of the middle 68% of the distribution. The typical error in \mathcal{M}/L_z is ± 0.4 , or $\sim 25\%$. These errors are propagated forward into mass-normalized quantities, although any possible variations in the IMF are not included.

All of the global galaxy properties discussed above are listed in Table 1, and all the quantities related to the globular cluster systems are presented in Table 2.

4. RESULTS

4.1. S_N versus Galaxy Magnitude

The historical definition of specific frequency, S_N , is the number of GCs per unit $M_V = -15$ of galaxy luminosity, or

$$S_N = N_{GC} \times 10^{0.4(M_V+15)} \quad (1)$$

(Harris & van den Bergh 1981). This number is approximately unity for the Milky Way. One of the motivations for calculating S_N is to understand whether GC formation scales with the bulk of star formation in the same way across galaxy types and masses. In Figure 2 we show the behavior of S_N as a function of M_V in our sample of 100 ACSVCS galaxies. The luminous early-type galaxies, mostly giant ellipticals, are well known to have $S_N \sim 2$ -5. The cD galaxy, M87, has $S_N = 12.6 \pm 0.8$ which is consistent with other measures of its S_N (e.g., Harris et al. 1998). Early-type galaxies of intermediate luminosity ($-22 < M_V < -18$) have a nearly uniformly low $\langle S_N \rangle \sim 1.5$. Galaxies in this luminosity range also have a tendency to be lenticular, with the VCC classifying 70% of these ACSVCS intermediate-luminosity galaxies as S0, E/S0 or S0/E. By contrast, the fainter galaxies ($M_V > -18$) exhibit a wide range of S_N , with values as low as zero and as high as those of M87¹⁹.

This trend has been hinted at previously from studies of giant ellipticals, lenticulars, and dwarf ellipticals. In Figure 3, we show the ACSVCS sample combined with data compiled from the literature. At the high luminosity end, we take S_N values from the compilation

¹⁹ Strader et al. (2006) analyzed a subset of these data and claimed a bimodal distribution of S_N in the dEs. A histogram of the S_N distribution shows that it is better described as strongly peaked with a tail to higher S_N , especially when one includes dS0s.

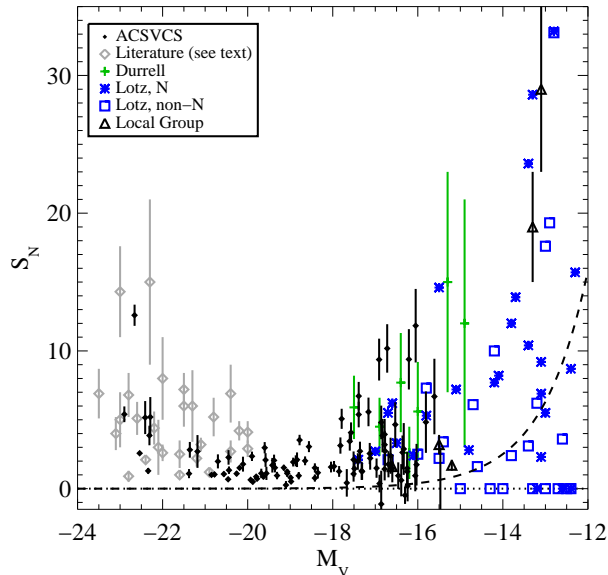


FIG. 3.— S_N versus galaxy M_V for 100 ACSVCS galaxies (black circles), and early-type galaxy data from the literature (references in the text). Literature values for S_N follow and extend trends visible in the ACSVCS galaxies. In particular, dwarf galaxy S_N values from the work of Durrell et al. (1996) and Lotz et al. (2004) show that fainter dwarf ellipticals can have an even larger range of specific frequency. For clarity, error bars are not plotted for the HST/WFPC2 dEs, but the uncertainty can be very large. The dashed line shows the S_N value if a galaxy at that magnitude had 1 GC.

of Ashman & Zepf (1998), using ones that were reliably determined from CCD data (gray diamond points). These include estimates from Kissler-Patig et al. (1996, 1997), Dirsch et al. (2003a, 2003b), Dirsch, Schubert & Richtler (2005), Forbes et al. (1996), Rhode & Zepf (2004), Zepf et al. (1995), and Harris, Harris & Geisler (2004). At the faint end, we include data from three sources which extend the range in galaxy luminosity by many magnitudes. We include the 7 dEs studied by Durrell et al. (1996a, 1996b) that do not overlap with our sample, the Virgo and Fornax dEs in the HST/WFPC2 study of Miller et al. (1998) and Lotz et al. (2004), and the five Local Group dwarfs listed in Lotz et al.

At the high luminosity end, the literature values have large scatter, possibly due to their heterogeneous nature. One of the benefits of the ACSVCS is that relative distances between Virgo cluster galaxies are both small and measured in a homogeneous fashion. At low luminosities, the studies are mainly in Virgo and Fornax so relative distances are less of a problem. At luminosities fainter than the ACSVCS, the trend of higher S_N coupled with a larger range of S_N continues to the limit of the data. The ACSVCS sample not only has smaller errors, it fills the important luminosity regime between giants and dwarfs. Kundu & Whitmore (2001a,b) studied galaxies in the magnitude range $-23 < M_B < -16$, similar to the ACSVCS, and found that ellipticals generally had higher S_N than lenticulars, but they were only able to measure “local” S_N within the WFPC2 field of view.

Ultimately, studies of GC specific frequency are about how GC formation scales with galaxy *mass*, using M_V as a proxy. However, a redder bandpass more faithfully

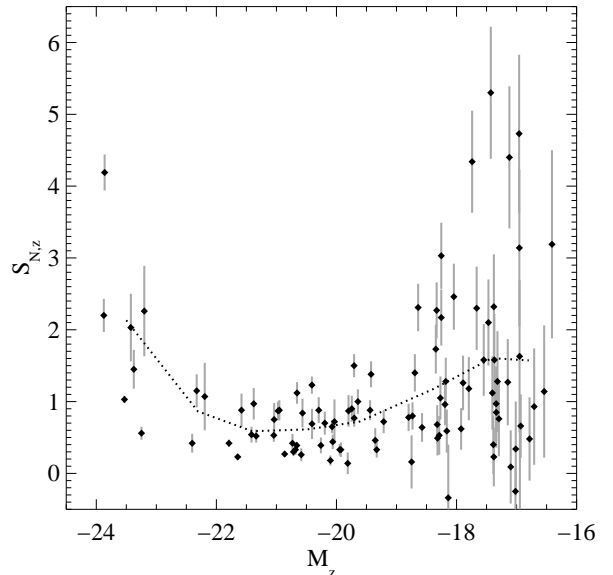


FIG. 4.— $S_{N,z}$ versus galaxy M_z . This figure shows similar quantities to those in Figure 2 except the number of GCs is normalized to the galaxy absolute magnitude in the z -band, with M_z is plotted along the x-axis. This far-red bandpass is a better tracer of the total stellar mass than the traditionally used V -band. The dotted line shows the mean trend with values in Table 4.

traces stellar mass, and in Figure 4, we introduce $S_{N,z}$, which is defined identically to S_N except that the number of GCs is normalized to an absolute z magnitude of $M_z = -15$, and plotted against M_z . $S_{N,z}$ values are 1.5 to 3 times smaller than S_N because early-type galaxies are red (and thus more luminous in z). The specific frequencies of giant ellipticals are adjusted more than those of the dwarfs because massive galaxies are redder in color. While the trends in this figure are the same as those in Figure 2, one interesting difference is that the highest $S_{N,z}$ values for the dwarfs now equal or exceed that of M87, with the change being due to M87’s redder color. For the rest of the paper, we will use quantities based on M_z .

4.2. $S_{N,z}$ and Bulge Luminosity

In most scenarios of GC system formation, the GCs are associated with the stellar spheroids—either halo or bulge—and not with the formation of present day disks. If this is the case, then perhaps normalizing GC numbers to total spheroid luminosity would be more fundamental than normalizing to total luminosity. In our ACSVCS sample, over half of our galaxies are morphologically classified in the VCC as either E/S0, S0/E, S0, or dS0. Most of these galaxies are at intermediate luminosities, and make up a substantial fraction of the galaxies that have low $S_{N,z}$. Could it be the case that these low $S_{N,z}$ values are due to the inclusion of a stellar disk in the total luminosity? Moreover, the scatter in the $S_{N,z}$ of the intermediate luminosity galaxies in our sample exceeds the scatter expected from the errors, implying that a parameter such as bulge fraction might be important.

We can test whether normalizing by bulge luminosity is more fundamental with quantitative bulge-disk decompositions (Chen et al., in prep). In this paper, however, we use the morphological T-types given in the Third Ref-

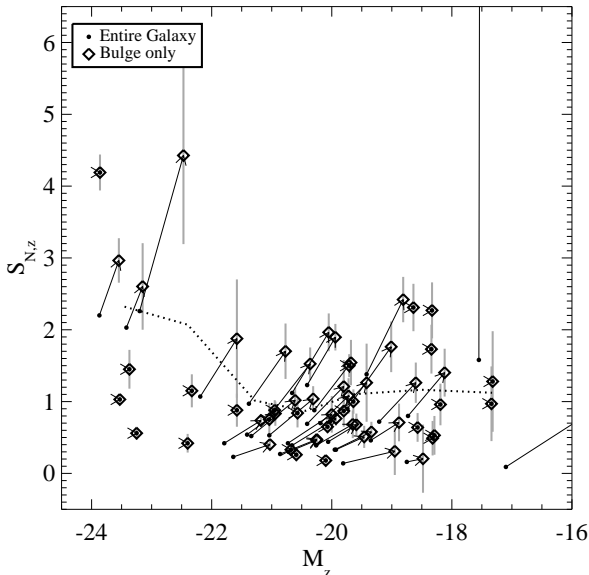


FIG. 5.— $S_{N,z}$ versus galaxy M_z for ACSVCS galaxies with VCC morphological types of E/S0, S0/E, S0, and dS0, and which have morphological T-types in the RC3. We plot the total $S_{N,z}$ (same as Figure 4) as well as an arrow connecting to the galaxy’s $S_{N,z}$ normalized to bulge luminosity alone. Some galaxies have $S_{N,z}$ similar to those in luminous ellipticals, but others are relatively unchanged.

erence Catalog of Bright Galaxies (RC3) (de Vaucouleurs et al. 1991). These T-types are correlated with the ratio of bulge to total luminosity using the relation of Simien & de Vaucouleurs (1986). We can do this for 55 galaxies in the ACSVCS sample and we show how their $S_{N,z}$ values change in Figure 5. This figure shows $S_{N,z}$ as derived using total luminosity compared to $S_{N,z}$ as derived from bulge luminosity alone with the two values connected by an arrow. For some galaxies, their specific frequencies do increase to values typical of the luminous ellipticals ($S_{N,z} \sim 1-2$), but for others whose disks are less prominent, their $S_{N,z}$ stay relatively unchanged. For two galaxies, their RC3 morphological types values imply that they have little or no bulge, which give them very high $S_{N,z}$.

Based on the current morphological classifications, it is not apparent that GCs form at a constant efficiency with respect to bulge luminosity. Normalizing to bulge luminosity increases the scatter in $S_{N,z}$ in the intermediate luminosity range. However, a more thorough analysis based on modern bulge-to-disk decompositions is necessary before we can reach any strong conclusions.

4.3. Normalizing to Stellar Mass

Using the stellar masses for the ACSVCS galaxies, we calculate the T parameter introduced by Zepf & Ashman (1993), which is the number of GCs (N_{GC}) per $10^9 M_\odot$,

$$T = N_{GC}/(\mathcal{M}_{G\star}/10^9 M_\odot) \quad (2)$$

where $\mathcal{M}_{G\star}$ is the stellar mass of the galaxy. The advantage of using T instead of S_N is that it allows comparisons across galaxies with different mass-to-light ratios. In Figure 6a and b, we show T plotted against M_z and

$\mathcal{M}_{G\star}$. Although the errors are larger than in Figure 4, the same trends are evident. Our values for T are higher than those in previous studies, such as Rhode & Zepf (2004). This is due to differences in the mass-to-light ratios used. Previous studies have assumed $\mathcal{M}/L_V = 10$ for elliptical galaxies, whereas we have estimated \mathcal{M}/L using galaxy colors and the BC03 models with a Chabrier (2003) initial mass function (IMF). Even accounting for the different bandpasses used, our \mathcal{M}/L are systematically lower. For example, for M49, the most luminous elliptical in the sample, $(V-z) = 0.97$ and its $\mathcal{M}/L_z = 2.0$ translates to $\mathcal{M}/L_V = 5$, which is a factor of two lower than the canonical Zepf & Ashman values. We feel that although the \mathcal{M}/L values in Zepf & Ashman (1993) have been valuable as standard conversions, they are too high, and that our values of \mathcal{M}/L are more reasonable given recent dynamical mass measurements of elliptical galaxies (Kronawitter et al. 2000; Cappellari et al. 2006). The use of a Salpeter (1955) IMF increases \mathcal{M}/L by a factor of 1.8, but is not observationally motivated for stars below $1 M_\odot$ and would produce stellar \mathcal{M}/L values higher than the total \mathcal{M}/L measured in some early-type galaxies. For the early-type galaxies in our sample, \mathcal{M}/L_V ranges from 1 to 5, although some galaxies with obvious star formation have $\mathcal{M}/L_V < 1$. We reiterate, though, that a using redder bandpass is better, and all our masses are derived using \mathcal{M}/L_z , and we discuss the V bandpass only for comparing with previous work.

For the purposes of this paper, however, the absolute scale of T is not as important as the relative scale within the sample. Figure 6b shows that T spans a wide range at masses $\mathcal{M}_{G\star} < 4 \times 10^9 M_\odot$, stays constant until $10^{11} M_\odot$, and then increases again at higher mass.

4.4. Specific Luminosity and Mass

If we want to know what fraction of a galaxy’s luminosity (or mass) is in GCs, we can total it up directly, as described in Section 3.2. We use the definition of specific luminosity, S_L presented in Harris (1991) except that we use the z bandpass instead of V :

$$S_{L,z} = 100 \times L_{GC,z}/L_{galaxy,z} \quad (3)$$

where $L_{GC,z}$ and $L_{galaxy,z}$ are the total z -band luminosities of the GCs and the galaxy. This quantity has two advantages over S_N in that it is independent of distance and that the completeness corrections for unobserved faint GCs are extremely small. We also plot the specific mass, S_M , defined as

$$S_M = 100 \times \mathcal{M}_{GC}/\mathcal{M}_{G\star} \quad (4)$$

where \mathcal{M}_{GC} is the total stellar mass in GCs, calculated as described in Section 3.2.

Figure 6c shows the specific luminosity S_L of GCs plotted against M_z , and Figure 6d shows S_M versus $\mathcal{M}_{G\star}$. The dashed line marks the 0.26% “universal” GC formation efficiency from McLaughlin (1999a), and is a reasonable description of the GC mass fraction in intermediate mass galaxies. For the ACSVCS galaxies with $-22 < M_z < -19$, $\langle S_L \rangle = 0.20$, $\sigma_{S_L} = 0.14$. Similarly, for galaxies with $\mathcal{M}_{G\star} = 0.4-6 \times 10^{10} M_\odot$, $\langle S_M \rangle = 0.17$, $\sigma_{S_M} = 0.11$. That the mass fraction is slightly lower than the luminosity fraction can be explained by the bluer colors and hence lower \mathcal{M}/L of the GCs as compared to their host galaxies.

TABLE 4
BINS OF M_z

M_z range	$\langle M_z \rangle$	$S_{N,z}$	T	S_L	S_M	$S_{N,z,blue}$	$S_{N,z,red}$	f_{red}	$S_{N,z,close}^1$	$S_{N,z,far}^2$
$(-25, -23)^3$	-23.4	1.6	13.2	0.90	0.74	1.17	0.47	0.29	1.72	1.57
$(-25, -23)$	-23.5	2.1	18.2	1.12	1.04	1.53	0.60	0.28	2.55	1.57
$(-23, -22)$	-22.3	0.9	8.5	0.51	0.50	0.49	0.37	0.43	1.11	0.43
$(-22, -21)$	-21.4	0.6	4.1	0.21	0.17	0.40	0.19	0.32	0.65	0.45
$(-21, -20)$	-20.5	0.6	4.7	0.18	0.16	0.43	0.19	0.31	0.57	0.68
$(-20, -19)$	-19.6	0.7	5.8	0.21	0.17	0.57	0.15	0.21	0.75	0.67
$(-19, -18)$	-18.4	1.2	11.4	0.38	0.34	0.99	0.18	0.16	1.41	0.80
$(-18, -17)$	-17.4	1.6	17.8	0.36	0.37	1.46	0.15	0.09	2.04	1.02
$(-17, -16)$	-16.8	1.6	17.3	0.51	0.35	1.36	0.21	0.13	2.03	...

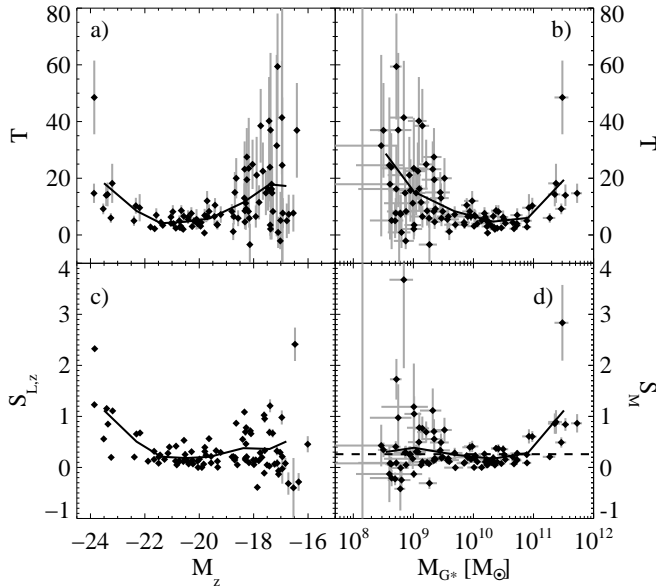
¹Within 1 Mpc of VCC 1316 (M87), in projection²Outside 1 Mpc of VCC 1316 (M87), in projection³Not including VCC 1316 (M87)

FIG. 6.— T_N versus M_z (a, upper left), and versus galaxy stellar mass (b, upper right). T_N is the number of GCs per $10^9 M_\odot$. In the bottom two plots we show the specific z luminosity, S_L , versus M_z (c, lower left) and the specific mass, S_M , versus stellar mass (d, lower right). The dashed line in (d) marks $S_M = 0.26$, the “universal” GC formation efficiency from McLaughlin (1999a). Because the ACSVCS sample is all early-types, M/L does not vary much, and hence in all four panels we see trends similar to those for S_N and $S_{N,z}$ (see text for exceptions). The difference between dwarfs and giants in S_L and S_M is not as large as it is in S_N or T_N . This reflects the changing GCLF across galaxy luminosity (see Figure 7). In all figures, the solid line shows the mean trend, values in Table 5.

The major difference in Figure 6 between the top two panels showing T (a and b) and the bottom two showing $S_{L,z}$ and S_M (c and d) is the comparison between the giants and dwarfs. While the dwarfs have very high number fractions, their luminosity and mass fractions are substantially lower compared to the giants. Why should this be the case? The reason for this has to do with the GCLF. If the GCLF was constant across all galaxies (i.e., same mean μ and width σ), then S_L would mirror T . However, Jordán et al. (2006, 2007) showed that the GCLF varies as a function of galaxy mass in the sense

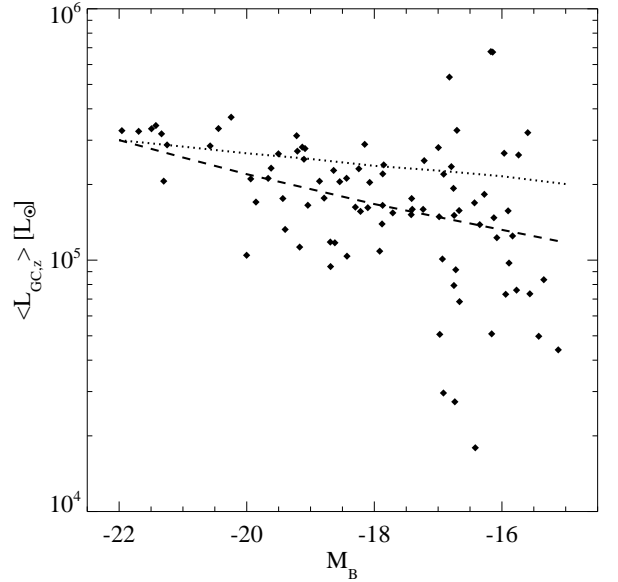


FIG. 7.— Mean z luminosity of GCs, $\langle L_{GC,z} \rangle$, in ACSVCS galaxies versus M_z . If the GCLF was constant across all galaxies, $\langle L_{GC,z} \rangle$ would also be constant. The affect of a fainter GCLF turnover in dwarf galaxies (dotted line) only partially explains the lower mean luminosities. A combination of fainter turnovers and narrower GCLFs (dashed line) reproduces the observed trend.

TABLE 5
BINS OF $M_{G\star}$

M_\star range ¹	$\langle M_\star \rangle^1$	T	S_L	S_M
(0.1, 0.5)	0.3	18.2	1.12	0.30
(0.5, 2.2)	1.0	8.5	0.51	0.39
(2.2, 10.0)	4.8	4.1	0.21	0.25
(10.0, 46.4)	21.1	4.7	0.18	0.17
(46.4, 215.4)	80.8	5.8	0.21	0.29
(215.4, 1000.0)	321.0	11.4	0.38	1.12
(215.4, 1000.0) ²	324.7	14.0	1.00	0.80

¹ $M_\star/10^9 M_\odot$ ²Not including VCC 1316 (M87)

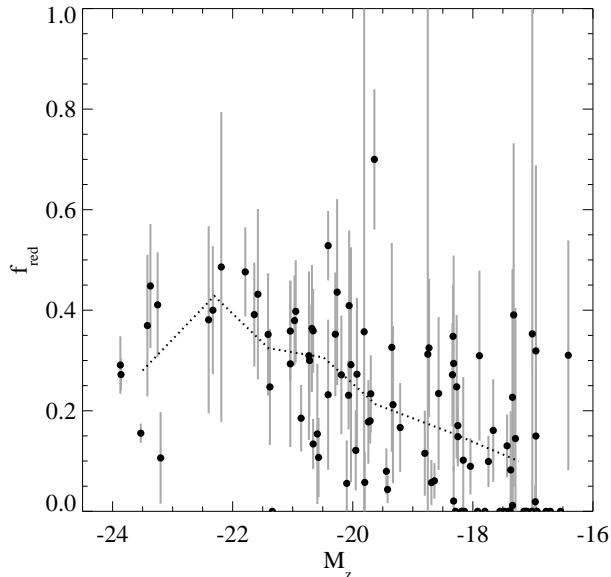


FIG. 8.— Fraction of red GCs (f_{red}) versus M_z . The dotted line represents the mean trend (Table 4). More luminous galaxies have higher fractions of red GCs up to $M_z \sim -22$, but at higher luminosities there is a flattening or turnover in f_{red} , and the most luminous galaxies do not have the highest red GC fractions.

that less massive galaxies host GC systems with fainter μ and smaller σ . This has the effect of lowering the mean luminosity (and mass) of GCs in the dwarf galaxies. We illustrate this in Figure 7, where we plot the mean z luminosity of GCs in each galaxy, $\langle L_{GC,z} \rangle$, against galaxy luminosity (in this case M_B because that is how we presented the data in Jordán et al.). It is clear that a constant GCLF does not describe the data well. The dotted line shows the effect of varying μ , and the dashed line shows the relation predicted by the combination of fainter μ and a narrower σ in the dwarfs. Although the scatter is large, the expected change in the GCLF can account for the changes in mean GC luminosity that we see. This trend is actually more pronounced in mass than in luminosity because GCs in dwarfs are more metal-poor and have lower M/L than those in giants.

The result is that some of the more extreme S_N or T values seen in the dwarfs are somewhat less extreme when expressed as a mass fraction. Nevertheless, many low-luminosity galaxies still have S_L and S_M that are significantly higher than those in the intermediate- L galaxies. Because the global trends are similar in S_N , T , S_L , and S_M , we will refer to these quantities collectively as “GC fractions”.

4.5. Specific Frequencies of Red and Blue GCs

Our previous study of GC color and metallicity distributions in the ACSVCS galaxies show that they are, on average, either bimodal or asymmetric across the entire luminosity range of the sample, and we use the products of that analysis (Peng et al. 2006a) in the current study. The blue (metal-poor) and red (metal-rich) are believed to trace either different epochs of formation or different progenitor halos (however, see Yoon, Yi & Lee 2006 and Cantiello & Blakeslee 2007 for arguments that the bimodality may be an observational consequence of a nonlinear metallicity-color relation). It is an interesting

question to ask how the specific frequencies of each GC population scale with galaxy properties. For example, Rhode & Zepf (2004) showed that the mass-normalized number of blue GCs, T_{blue} , increases as one goes from spirals to elliptical galaxies, although their spirals were less massive than ellipticals so the trend could also have been one in galaxy mass. Assuming that mergers of spirals only produce new red GCs, they argued that the GC systems of ellipticals cannot be formed purely by spiral mergers.

We determine the fraction of blue and red GCs in a hybrid approach similar to what we do for total numbers. For the brightest 21 galaxies in the sample (a complete magnitude-limited sample, as ranked by B_T in Côté et al. 2004; Paper I) there are sufficient numbers of GCs that the KMM two-Gaussian fits to the $(g-z)$ distribution performed by Peng et al. (2006a; Paper IX) are reliable enough that we can use the “dip” between the two Gaussians—the color at which a GC is equally likely to belong to the blue or red GC distribution—as the dividing color between the two populations. For the remaining galaxies, we assume a fixed dividing color of $(g-z) = 1.16$. Although the colors of the individual peaks vary as a function of galaxy luminosity, the dip color is relatively invariant (see Figure 5 in Peng et al. 2006a).

The brighter galaxies may have better defined color distributions, but we only observe a fraction of their entire GC system, and the red-to-blue ratio is observed to decrease as a function of galactocentric radius. We correct for this bias in the brightest 14 galaxies by fitting Sérsic models to the surface density profiles of the red GCs separately, and integrating the best model to obtain their total numbers. We fit to profiles derived from our ACS and WFPC2 data, as described in §3.1. In the most luminous galaxies such as M49 and M87, the fraction of red GCs within the ACS/WFC is as high as 0.6, but the red fraction of the entire GC system is more like 0.3. For the remainder of the galaxies, we find that the ACS/WFC encompasses nearly all of the red GC system and use our corrected counts to determine the red GC fraction.

Figure 8 shows the fraction of red GCs as a function of M_z . The fraction of red GCs, f_{red} , generally increases with galaxy luminosity, going from ~ 0.1 to ~ 0.5 , but at $M_z \lesssim -22$, the trend in f_{red} appears to either flatten or perhaps turn over. This is in contrast to the results of Paper IX which only quantified the red GC fraction within the ACS/WFC images, and thus were biased to detecting the more centrally concentrated red GCs. With the proper aperture corrections, we can see that the most luminous galaxies in the sample do not have increasingly higher fractions of red GCs. Is this because there are fewer red GCs in these galaxies or more blue GCs?

Figure 9 shows the $S_{N,z}$ for blue and red GCs as function of M_z . The trend in the blue GCs mirrors the overall trend seen in Figure 4, with the massive and dwarf galaxies having the highest $S_{N,z}$. This is not surprising on the faint end since most of the GCs in the fainter galaxies are blue. Even for the massive galaxies, the high $S_{N,z}$ values are dominated by blue GCs. However, the specific frequencies of red GCs also exhibit an increase for $M_z < -21$, especially for the cD galaxy M87, which is a 4σ outlier. The elevated $S_{N,z,blue}$ and $S_{N,z,red}$ for the most massive galaxies, suggests that massive galaxies are

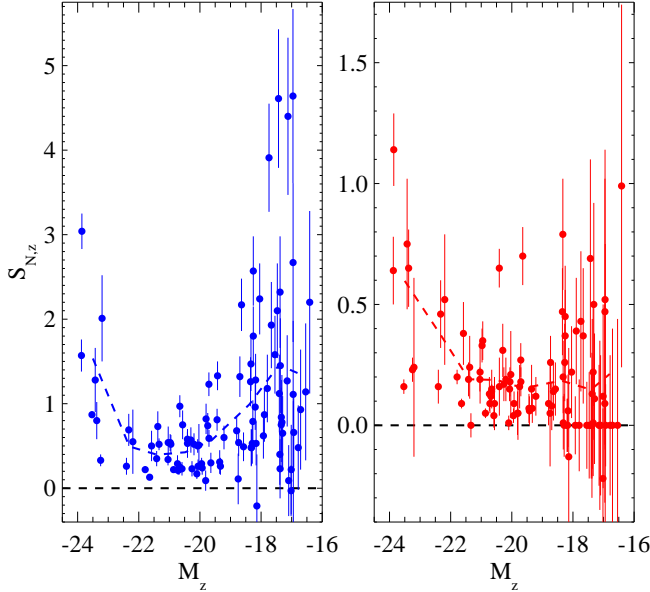


FIG. 9.— $S_{N,z}$ versus M_z for blue (left) and red (right) globular clusters. Both red and blue GCs show enhanced $S_{N,z}$ in massive galaxies, but the variation in $S_{N,z}$ across galaxy mass is dominated by the blue GCs. This is true even in the massive galaxies. The dashed lines show the mean trends with values listed in Table 4.

not underproducing red GCs, which is one possible interpretation of Figure 8. Instead, these massive galaxies have more red GCs, but even more blue GCs.

4.6. $S_{N,z}$ and Nucleation

Observations by the HST/WFPC2 of dEs in the Virgo and Fornax Clusters (Miller et al. 1998; Lotz et al. 2004; Miller & Lotz 2007) have found that dEs with stellar nuclei have a higher mean specific frequency, possibly implying that a higher past star formation efficiency resulted in the formation of both nuclei and GCs. The dEs in our sample are more luminous than the ones studied in the WFPC2 snapshot survey, and almost all of the galaxies are nucleated (Côté et al. 2006; Paper VIII). Therefore, it is difficult to test if there is any correlation between $S_{N,z}$ and nucleation. Only four dwarf galaxies are definitely non-nucleated (Type II in Table 1 of Paper VIII)—VCC 1049, 1833, 1499, and 1512. Of these galaxies, VCC 1499 and 1512 are dE/dI transition objects with young stars, and VCC 1049 has bluer colors toward the center. The $S_{N,z}$ values of these galaxies range from 0.97 (VCC 1049) to 3.14 (VCC 1499) and do not appear different from the rest of the sample. When normalized to stellar mass, however, the young stellar populations have lower M/L and thus much higher T and S_M values.

4.7. $S_{N,z}$ and Environment

One of the more intriguing questions presented by plots such as Figure 4 is the nature of $S_{N,z}$ in the low-luminosity galaxies ($M_z > -19$), which we will loosely refer to as “dwarfs”, although some of the galaxies in our sample are on the more massive end of the spectrum of dwarf galaxies. Our relatively small errors show that the large spread in specific frequency for dwarf galaxies is not

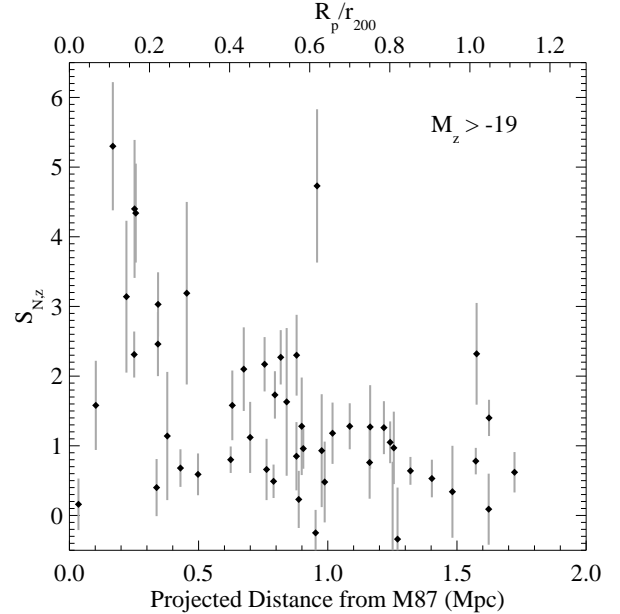


FIG. 10.— $S_{N,z}$ vs projected clustercentric distance for low-luminosity galaxies ($M_z > -19$), excluding VCC 571 and 538 which are known to be $\sim 6-7$ Mpc behind the Virgo core (Mei et al. 2007). The center of the Virgo cluster is taken to be the location of the cD galaxy, M87, and the top axis shows R_p/r_{200} where $r_{200} = 1.55$ Mpc. There is a notable trend in specific frequency with clustercentric radius. All but one galaxy with $S_{N,z} > 2$ are within $R_p \sim 1$ Mpc of the cD.

TABLE 6
BINS OF R_p FOR GALAXIES WITH $M_z > -19$

R_p range Mpc	$\langle R_p \rangle$ Mpc	$S_{N,z}$	T	$S_{N,z,blue}$	$S_{N,z,red}$
(0.00, 0.15)	0.07	0.47	3.9	0.40	0.07
(0.15, 0.30)	0.23	3.46	33.3	3.17	0.29
(0.30, 0.50)	0.40	1.58	15.7	1.34	0.23
(0.50, 1.00)	0.83	1.38	13.0	1.14	0.23
(1.00, 1.50)	1.24	0.70	8.4	0.59	0.11
(1.50, 2.00)	1.62	1.05	11.6	0.99	0.06

simply due to the expected observational scatter. Given our errors, the observed distribution of $S_{N,z}$ is 2.4 times broader than we would expect if all dwarfs had a single $S_{N,z}$. This implies that there is at least one other parameter besides galaxy mass that governs the GC formation efficiency.

In this section, we investigate the relationship between specific frequency and the galaxy’s environment—specifically, its distance from the cluster center, which is taken to be the location of the cD galaxy, M87 (Binggeli et al. 1985). Environment clearly plays a role in galaxy evolution, as is evidenced by the morphology-density relation, and this can be through gravitational and hydrodynamic processes such as tidal and ram pressure stripping, or through initial conditions where halos in denser regions collapse earlier. Dwarf galaxies, being the most vulnerable, are more likely to express the effects of their environment.

Figure 10 shows $S_{N,z}$ for dwarf galaxies against their projected distance from the cluster center (R_p), ignoring

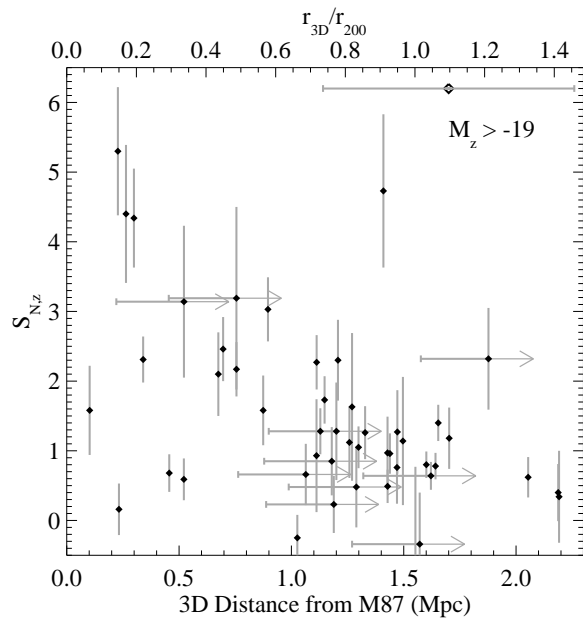


FIG. 11.— S_N versus three dimensional clustercentric distance for low-luminosity galaxies ($M_z > -19$). The top axis shows R_{3D}/r_{200} where $r_{200} = 1.55$ Mpc. The error bar at top right shows the mean distance error. Points with arrows do not have SBF distances so we have used their projected distances and added 0.3 Mpc (the median $(R_{3D} - R_p)$ for the rest of the sample). The left error bar is at their projected radii, and are thus lower limits on their 3-d radii.

TABLE 7
BINS OF R_{3d} FOR GALAXIES WITH $M_z > -19$

R_{3d} range Mpc	$\langle R_{3d} \rangle$ Mpc	$S_{N,z}$	T	$S_{N,z,blue}$	$S_{N,z,red}$
(0.00, 0.25)	0.19	1.38	11.3	1.19	0.18
(0.25, 0.50)	0.34	2.39	23.9	2.19	0.20
(0.50, 1.00)	0.71	2.13	20.8	1.87	0.26
(1.00, 1.50)	1.27	1.27	13.5	1.05	0.22
(1.50, 2.00)	1.65	0.78	7.7	0.68	0.10
(2.00, 2.50)	2.14	0.50	5.2	0.47	0.03

VCC 571 and 538 which are known from their SBF distances to lie 6–7 Mpc behind the cluster core (Mei et al. 2007). There is a remarkably clear correlation in which dwarfs closer to M87 have higher $S_{N,z}$. Of the 14 galaxies with $S_{N,z} > 2$, 13 lie within a projected radius of 1 Mpc (the exception being VCC 21, a possible dE/dI transition galaxy). We note that this is roughly half of r_{200} for the Virgo A subcluster centered on M87 (McLaughlin 1999b; Côté et al. 2001), where $r_{200} = 1.55$ Mpc is the radius at which the mass density of M87 is 200 times the critical density. This value has been recalculated for $D_{M87} = 16.5$ Mpc using the McLaughlin (1999a) model (D. McLaughlin, priv. comm.). When we plot $S_{N,z}$ against three-dimensional clustercentric distance (Figure 11), we see the same trend although the error in the line-of-sight distance introduces more scatter. Tables 6 and 7 list the values for the mean trends in these Figures.

The M87 globular cluster system is one of the most extreme in the local supercluster and it is possible that some of the M87 halo GCs, or a population of intra-

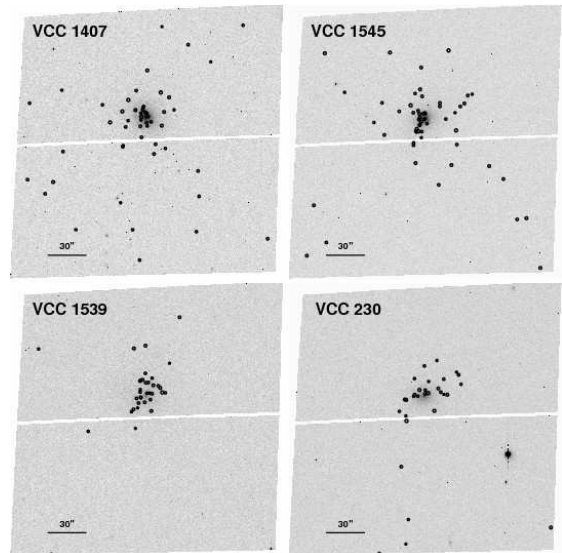


FIG. 12.— Spatial distributions of GC candidates (circles) in 4 dEs with the highest specific frequencies (VCC 1407, 1545, 1539, and 230). In all cases, there is evidence of a rich GC system that is centrally clustered around the galaxy, showing that their elevated S_N is not due to an enhanced level of interloping GCs from the cD galaxy or an intracluster population. These galaxies have $\sim 5\times$ more GCs than “normal” galaxies with $S_{N,z} = 1$. The images show the entire ACS field of view, and the scale bar in the lower left of each image has a length of $30''$. The blank diagonal strip is the gap between the two ACS CCDs. Catalogs have been statistically cleaned using expected contamination determined from control fields.

cluster GCs, are contaminating the GC systems of the nearby dwarfs. In fact, the five galaxies closest to the cD, VCC 1297, 1327, 1279, 1250, and 1185 have been treated differently in our analyses in this paper because it is obvious that some to all the GCs detected are part of the M87 halo. One of the telltale signatures of this is whether the GCs are uniformly distributed across the ACS/WFC image rather than centrally concentrated around the targeted galaxy. Figure 12 shows the locations of GC candidates around the 4 dEs with the highest $S_{N,z}$. In all cases, the star clusters are concentrated toward the center of the galaxy and not in a uniform spatial distribution. An extension of the M87 GC radial density profile using a Sérsic model fit to the ACSVCS data and the ground-based data of McLaughlin (1999) (see Figure 1) predicts only 1–3 M87 GCs over the entire ACS/WFC field of view at the distances of VCC 1407, 1545, and 1539. The GC radial profile from Tamura et al. (2006) gives slightly higher values, with an expected 9^{+3}_{-6} M87 GCs in the ACS field at the projected distance of VCC 1407, a dE which has 50 GCs. Given the difficulties in measuring the M87 GC density from ground-based data, especially given uncertainties in background subtraction, these independent estimates are consistent. Extrapolations of a de Vaucouleurs profile fit to the Tamura et al. data predict ~ 2 M87 GCs in the ACS fields for VCC 1545 and 1539. We also have a parallel WFPC2 observation at a distance of $40'$ from M87 in which we find a number of GCs consistent with zero. Finally, as these galaxies have 31–54 GCs each, this contamination from M87 GCs is expected to be *at most* 6–18%.

The general trend of dEs having higher $S_{N,z}$ is reversed for the two dwarfs (VCC 1297 and 1185) with $R_p \lesssim 100$ kpc. These galaxies have low intrinsic numbers of

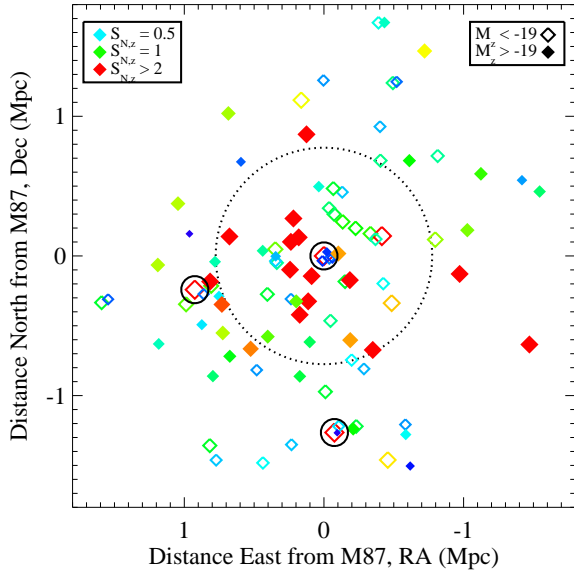


FIG. 13.— Spatial distribution of ACSVCS galaxies color coded by $S_{N,z}$. Specific frequency increases as colors change from blue to red. Filled points are dwarfs ($M_z > -19$) and open points are the more luminous galaxies. The three large solid circles represent the three massive ellipticals in the Virgo cluster: the cD galaxy M87 center, M49 bottom, and M60 (VCC1978/N4649) left. The large dotted circle represents $r_{200}/2 = 775$ kpc for the M87/Virgo A subcluster. The high $S_{N,z}$ galaxies are preferentially around the cD, while no enhancement appears around the cluster’s most luminous galaxy M49. Dwarfs immediately in the vicinity of the giants have low $S_{N,z}$ and may be tidally stripped.

GCs and we hypothesize that they have had their GCs stripped from them by M87. Both VCC 1297 and the more luminous VCC 1327 are within $R_p \approx 40$ kpc, and have GC numbers consistent with zero. The galaxies VCC 1192 and 1199, which are at comparable distances from M49, also have undetectable intrinsic GC systems.

Figure 13 shows the positions of the ACSVCS galaxies on the sky, color and size coded by $S_{N,z}$, with open points representing giants and filled points for dwarfs. The high- $S_{N,z}$ dwarfs are clustered around M87, and there is no similar effect around the brightest galaxy in the cluster, M49, nor around VCC 1978 (M60/N4649). Interesting exceptions are the aforementioned galaxies within the immediate vicinities of the giants ($R \lesssim 40$ kpc), which have few or no GCs and may have been tidally stripped of their GC systems. The specific frequencies of the more massive galaxies are generally uniform, as shown in Figure 4, and thus are relatively unaffected by their distance from M87.

We can re-plot Figure 4, except divided into two samples, one inside and one outside a projected clustercentric distance of 1 Mpc. Figure 14 shows the difference between the two samples. Galaxies within 1 Mpc mirror the trends seen in Figure 4, with both giant and dwarf galaxies having high $S_{N,z}$. However, the sample of galaxies outside of 1 Mpc entirely lacks high- $S_{N,z}$ dwarfs. The division is not perfect, as there are still low- $S_{N,z}$ dwarfs within 1 Mpc (some of which have larger 3-D distances), but the lack of high- $S_{N,z}$ dwarfs on the outskirts of the cluster or around the other massive ellipticals is very clear. The one possible exception to the general trend is VCC 230, which lies at $R_p = 0.96$ Mpc and has an

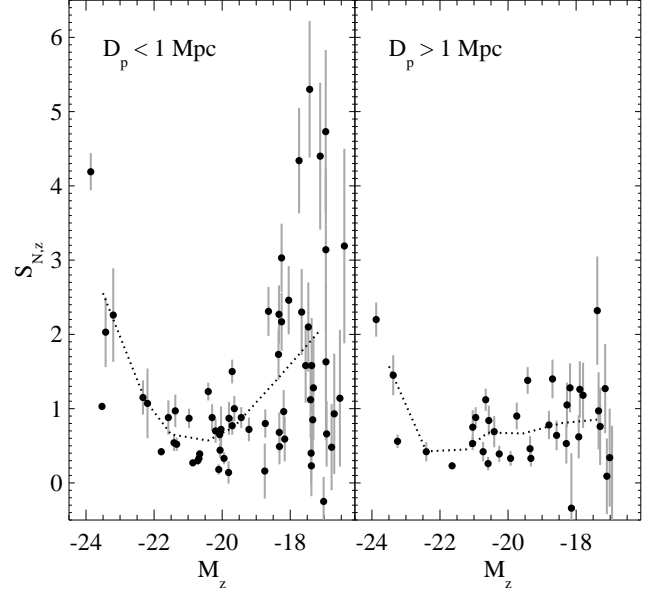


FIG. 14.— $S_{N,z}$ versus galaxy M_z , as in Figure 4, except divided by clustercentric distance. Galaxies within 1 Mpc of the cluster center exhibit the full range of $S_{N,z}$, but nearly all the dwarfs outside of 1 Mpc have low specific frequencies ($S_{N,z} \leq 1.5$). The only exception is a dE/dI transition object (VCC 21).

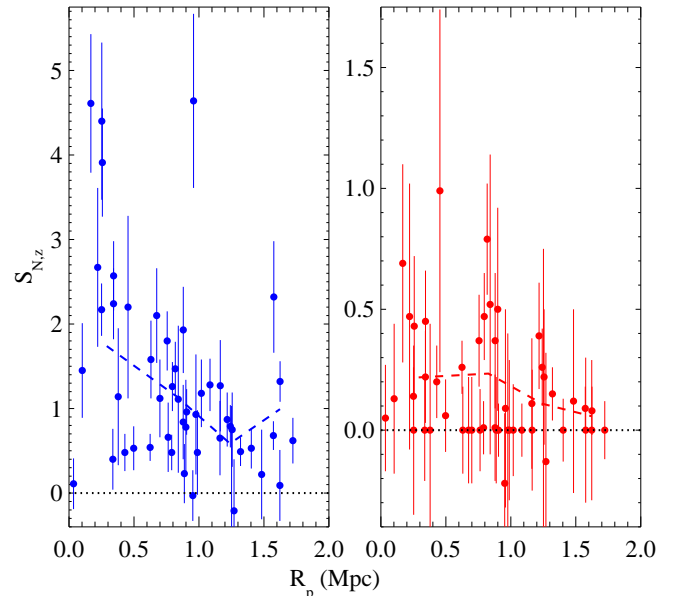


FIG. 15.— $S_{N,z}$ versus projected clustercentric distance for blue GCs (left) and red GCs (right) in low-luminosity galaxies ($M_z > -19$). Given that most GCs in dwarfs are metal-poor, it is not surprising that the trend for blue GCs mirrors that in Figure 10. The $S_{N,z}$ for the red GCs may also show a tendency to be enhanced at small clustercentric radii, but the numbers involved are small.

$S_{N,z}$ higher by a factor 2 than other galaxies at comparable distances.

The GCs in dwarf galaxies are predominantly from the blue (metal-poor) subpopulation, but many in the ACSVCS sample also possess small numbers of red GCs. Are both of these subpopulations affected by environment? In Figure 15, we plot $S_{N,z}$ in dwarf galaxies against R_p for the blue and red GCs separately. As expected, the blue GCs mirror the overall trends since they

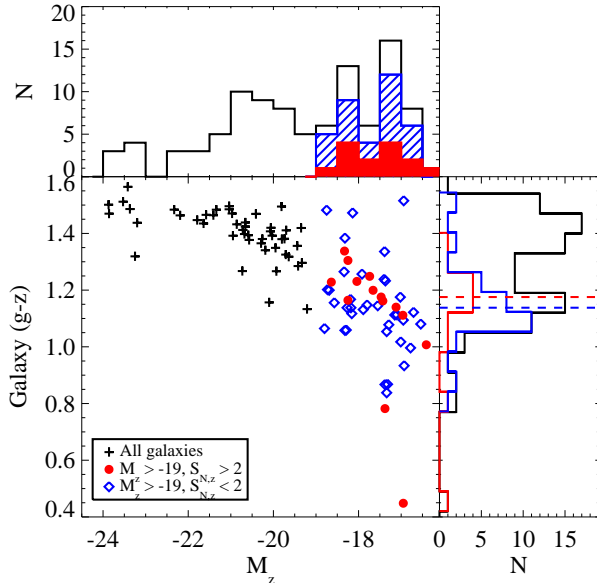


FIG. 16.— Color-magnitude properties of dwarfs with high and low $S_{N,z}$. We show $(g-z)$ vs. M_z and accompanying histograms for the ACSVCS sample of galaxies. Galaxies with $M_z > -19$ are separated at $S_{N,z} = 2$. The luminosity distribution of the two subsets are nearly identical, while the high- $S_{N,z}$ dwarfs have a median color that is formally redder than that of the low- $S_{N,z}$ dwarfs (shown by dashed lines in right hand histogram).

dominate the GC budget. For the red GCs, although the errors are large, there is a slight hint that dwarfs with smaller clustercentric distances tend to have elevated red GC specific frequencies. The mean $S_{N,z,red}$ of dwarfs within 1 Mpc is 0.2, compared to 0.1 for those outside.

Do the dwarfs with higher $S_{N,z}$ exhibit any intrinsic characteristics that differentiate them from the others? Figure 16 shows the $(g-z)$ - M_z color-magnitude diagram for the ACSVCS galaxies, singling out the dwarfs with both low and high $S_{N,z}$, and dividing the sample at $S_{N,z} = 2$. The top histogram plots the M_z distribution of the total, high- $S_{N,z}$, and low- $S_{N,z}$ samples and shows how the luminosity distributions of the two groups are nearly identical. On the right-hand histogram, we plot the color distribution with the median colors marked by the dashed lines. Although the high- $S_{N,z}$ dwarfs formally have redder colors, $\Delta(g-z) = 0.05$ mag, the difference is not significant. We have also investigated possible differences in their structural properties (Sérsic n , r_e) as well as in the colors of their globular clusters, and for none of these properties are high- $S_{N,z}$ dwarfs significantly different from low- $S_{N,z}$ dwarfs.

5. DISCUSSION

5.1. Mass Dependence of the GC Mass Fraction

Globular cluster specific frequency and its related quantities are clearly dependent on the mass of the host galaxy. However, GC fraction does *not* vary monotonically with galaxy mass, making it unlike most other properties measured for the ACSVCS galaxies—e.g., colors, structural parameters (Ferrarese et al. 2006a), core deficit and excess (Côté et al. 2007), GC mean colors (Peng et al. 2006a), GC mean sizes (Jordán et al. 2005), and GC luminosity function parameters (Jordán et al. 2007). These papers (particularly Papers VI and VIII)

show that there is no clear distinction between “dwarfs” and “giants”, and that early-type galaxy properties have a smooth, monotonic dependence on galaxy mass. For GC fractions, however, a transition does appear to exist.

It is possible that GC fraction is telling us more about the variable formation efficiency of stars in the field than it is about the formation of GCs themselves. Blakeslee et al. (1997), Blakeslee (1999) and McLaughlin (1999a) have shown that, at least on the high mass end, the number of GCs appears to scale directly to the baryonic, or even the total mass. Kravtsov and Gnedin (2005) show a similar relation in their simulations of GC formation. High S_N values may then be interpreted as a lower fraction of baryons that form field stars.

The mismatch between total mass and stellar mass across the galaxy mass function is now well known in the study of galaxy formation. Observationally, dynamical mass estimates of galaxies across a wide range of mass require high mass-to-light ratios for both high (Côté et al. 2001, 2003) and low mass galaxies (Mateo 1998), with low \mathcal{M}/L measured for galaxies around L^* (Romanowsky et al. 2003; Peng et al. 2004; Napolitano et al. 2005). Mass-to-light ratios for ensembles of galaxies derived from weak lensing have also produced similar trends in \mathcal{M}/L (e.g., Guzik & Seljak 2002; Hoekstra et al. 2005; Mandelbaum et al. 2006). One can also take a statistical approach and match the expected dark matter halo mass distribution from simulations and the observed galaxy luminosity function (Berlind & Weinberg 2002; van den Bosch et al. 2003, 2007; Vale & Ostriker 2007), which does not require us to know the details of galaxy formation. These halo occupation studies infer a maximum conversion efficiency of baryons to stars at halo mass $\mathcal{M}_h \sim 2 \times 10^{11} \mathcal{M}_\odot$, or a stellar mass of $\mathcal{M}_{G\star} \sim 7.5 \times 10^9 \mathcal{M}_\odot$. In simulations of galaxy formation, this $\mathcal{M}_h/L-L$ relation (or alternatively, $\mathcal{M}_h/\mathcal{M}_{G\star}-\mathcal{M}_{G\star}$) requires various heating mechanisms (photoionization, stellar and AGN feedback) to prevent the formation of more stars in galaxies than are observed (Benson et al. 2002; Croton et al. 2006).

What happens if we make the simple assumption that $N_{GC} \propto \mathcal{M}_h$, or equivalently $S_{\mathcal{M}} \propto \mathcal{M}_h/\mathcal{M}_{G\star}$? Ideally, we would know the total dynamical mass of each galaxy in our sample. Without this information, we can apply average halo mass-to-light ratios derived from the halo occupation studies, in this case using the parameterization of van den Bosch et al. (2007) and a WMAP3 cosmology (Spergel et al. 2007). We transform their L_B to $\mathcal{M}_{G\star}$ using a range of $\mathcal{M}_{G\star}/L_B$, monotonically increasing from 1.8 to 4.1 as a function of galaxy luminosity, derived from a polynomial fit to the inferred $\mathcal{M}_{G\star}/L_B$ and measured L_z of the ACSVCS galaxies. This results in a simple prediction for the behavior of $S_{\mathcal{M}}$ as function of galaxy stellar mass.

In Figure 17, we plot the ACSVCS data for $S_{\mathcal{M}}$ against $\mathcal{M}_{G\star}$ with errors for both $S_{\mathcal{M}}$ and $\mathcal{M}_{G\star}$. We extend the data to lower mass galaxies by including the Virgo and Fornax dEs and five Local Group dEs from Lotz et al. (2004). For these latter data, we assume $\mathcal{M}_{G\star}/L_B \sim 2.5$ (an extension of the mass-to-light ratios fitted to the ACSVCS dwarfs) and $\langle \mathcal{M}_{GC} \rangle = 1.6 \times 10^5 \mathcal{M}_\odot$, the mean GC mass in our ACSVCS dwarfs. The Virgo and Fornax dE points do not include errors in their stellar masses, and for the Local Group dEs, we have assumed

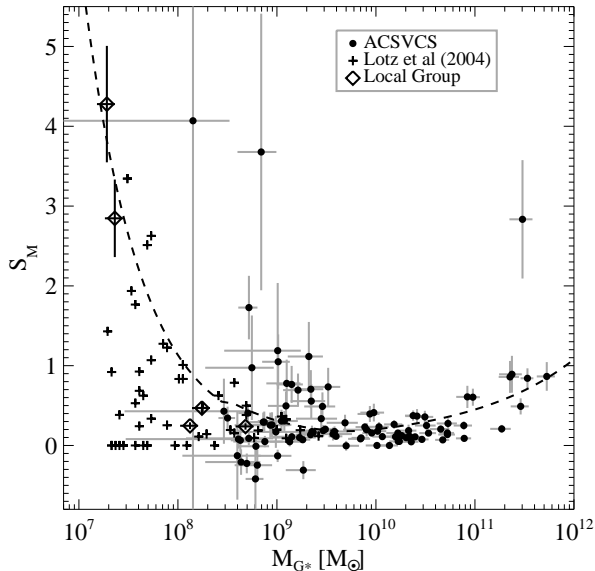


FIG. 17.— Mass fraction of GCs, S_M , versus galaxy stellar mass M_{G^*} for ACSVCS galaxies (filled dots), Virgo and Fornax dEs from Lotz et al. (2004) (crosses), and Local Group early-type dwarfs (diamonds). We overplot the expected behavior of S_M assuming that the mass in GCs follows the total halo mass as inferred from the $M_h/L-M_h$ relation of van den Bosch (2007). This assumption can explain the rise in S_M for luminous galaxies, although the cD galaxy M87 is off the relation because its stellar mass is not representative of its halo mass. At the low mass end, we also expect a sharp rise in S_M which is traced by some cluster and Local Group dEs. At masses of $\sim 10^9 M_\odot$, however, many dEs in the ACSVCS sample have higher S_M than might be expected. The high- S_M and low- S_M dwarfs cannot be explained simultaneously if GC mass fraction is solely a function of galaxy stellar mass.

an error in their luminosities of 0.25 mag. Overplotted on the data is the predicted behavior of S_M assuming $S_M \propto M_h/M_{G^*}$. The only truly free parameter in the plot is the vertical normalization, which is chosen to match both the massive elliptical M49 and the Local Group dwarf spheroidal galaxies Fornax and Sagittarius. The assumption that the GC mass fraction is proportional to the inverse of the stellar mass fraction, $S_M \propto M_h/M_{G^*}$ predicts that S_M should be high at both high and low masses. At high stellar masses, the rise reflects the increasing M/L of massive elliptical galaxies. One galaxy, M87, is well off the predicted relation, but this is because its GC population is more likely representative of the entire Virgo A subcluster within which M87 resides (McLaughlin 1999a). The sharp cutoff in the galaxy luminosity function and the nearly universal luminosity of brightest cluster galaxies means that S_M can vary widely depending on whether the luminosity is associated with a galaxy halo or the cluster halo (Blakeslee 1999, Jordán et al. 2004a). At low masses, S_M is also predicted to rise steeply, but this is at masses lower than those in our sample. Many of the ACSVCS dwarfs around $M_{G^*} \sim 10^9 M_\odot$ have S_M higher than we would infer by a factor of 4–8, and these are the same ones that are in the inner regions of the Virgo cluster. At masses below $M_{G^*} \sim 10^8 M_\odot$, the dEs from Lotz et al. (2004) are either consistent with or below the expected rise, although the observational error is quite large (and not shown for clarity). So, while the linear scaling of

$M_{GC} \propto M_h$ does seem to be relevant to S_M across a large galaxy mass range, the S_M for the ACSVCS dwarf galaxies in this diagram is not explained by a dependence on galaxy mass alone. The scatter in S_M for dwarfs (and also possibly for intermediate mass galaxies) also cannot be explained by the intrinsic scatter in galaxy M/L (from van den Bosch et al. 2007). The scatter is even harder to explain for S_L where the errors are considerably smaller.

Both Forbes (2005) and Bekki, Yahagi & Forbes (2006) have also attempted to explain the increase in S_N for dwarf galaxies by assuming a relation between GCs and galaxy mass. These attempts followed similar arguments by Durrell et al. (1996) and McLaughlin (1999a). Forbes (2005) used the data for ACSVCS galaxies presented in Peng et al. (2006a, Paper IX) to compare the approximate S_N of blue GCs in dwarf galaxies with the scaling relation of Dekel & Birnboim (2006), where $M/L_V \propto M^{-\alpha}$. Forbes (2005) use $\alpha = 2/3$ from Dekel & Birnboim (2006) for masses below the critical galaxy stellar mass of $3 \times 10^{10} M_\odot$ where galactic winds should be more efficient at blowing gas and metals from the galaxy (Kauffmann et al. 2003; Tremonti et al. 2004). They also assume a constant number of GCs as a function of galaxy mass, giving $S_N \propto M^{-5/3}$. Although this formulation predicts a rapid rise in S_N and S_M for fainter galaxies, it is much too steep to accommodate the data in the way that they present it. The normalization of this relation as presented in Forbes (2005) is not constrained, but because the relation is steep, the normalization is critical for comparing to the data. If we fix to the mean S_M at the critical mass, the relation overpredicts S_M for all the dwarfs. This is due to the fact that dwarf galaxies do not have a constant number of GCs. Bekki et al. (2006) simulate GC systems and test various values for α , concluding that the observations are not consistent with $\alpha = 0$ (a constant M/L), and it would be interesting to determine α again with this new data set. Whatever the best value of α , however, a simple relation where the specific frequency is determined solely by the present day stellar mass of a galaxy is unable to describe all of the data on the low mass end.

5.2. Environment and Biased GC Formation

5.2.1. Cluster Dwarfs in the Millennium Simulation

As we showed in Figures 10-15, GC specific frequency is not purely a function of galaxy mass, but can also depend on environment. We do not see environmental effects on S_N for massive galaxies with the exception of M87, whose location defines the cluster center. For intermediate-mass galaxies in particular, S_N does not appear to depend on environment. For dwarf galaxies, however, specific frequency is a strong function of proximity to the center of the Virgo Cluster. Nearly all dwarfs with high S_N are within $R_p = 1$ Mpc.

One of the main problems with building up the blue GC sub-population in the halos of massive galaxies is that the ratio of metal-poor GCs to metal-poor field stars in galaxies is very high (Harris & Harris 2002). In other words, if halos are built up through the accretion of dwarf galaxies or dwarf-mass fragments then their specific frequencies need to be high in order to keep the main body of the galaxy metal-rich. These central dwarfs with high

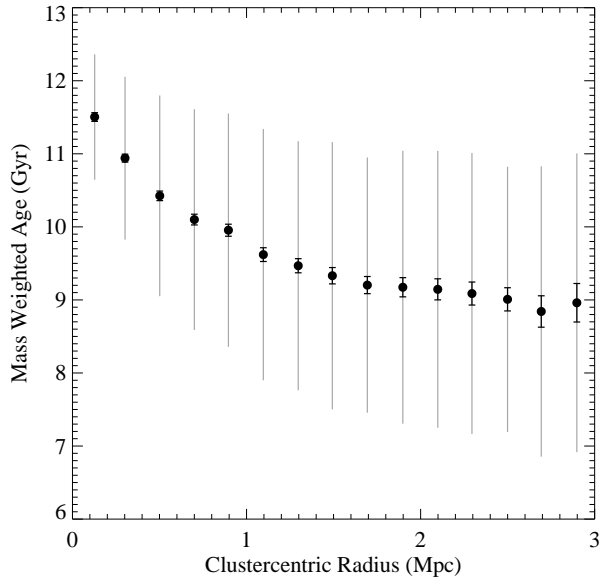


FIG. 18.— The mass-weighted stellar age of low mass ($M_z > -19$) early-type cluster galaxies in the Millennium Simulation. Galaxies in the inner regions of the galaxy cluster have older mean ages. The black error bars with hats depict the 2σ error in the mean, while the gray error bars indicate the 1σ width of the age distribution in each bin.

S_N may then hold the key to the formation of GC systems, as they are likely to be most similar to the progenitors of any dwarfs that have since merged into the halo of M87. Figure 9 shows that the $S_{N,z,blue}$ values for the innermost dwarfs are as high or higher than that of M87 or any of the other giant ellipticals. These dwarfs could be the survivors of an accreted population of protogalaxies that may have had even higher GC mass fractions and redder GCs. In fact, the two galaxies closest to M87—VCC 1327 and 1297—have GC systems that are either entirely stripped or undetectable against the M87 GC system, and their $g-z$ colors are much redder than those of other galaxies with the same luminosity (see the red outliers in Figure 16).

What is the cause of the enhanced GC fractions in these central dwarfs? Are they more efficient at producing GCs for their mass, less efficient at forming field stars, or better at keeping the GCs they form? As discussed earlier, one possible way for GC production to be biased towards the central dense regions of the galaxy cluster is for these galaxies to form a larger fraction of their stars earlier and at a higher star formation rate density. Although we do not currently have the ability to determine the detailed star formation histories of the ACSVCS galaxies at these early times, we can use simulations to study global trends in the star formation histories of low mass early-type galaxies in the cluster environment. By using simulations, we can test the consistency of the hypothesis that the central dwarfs must be both older and have higher SFR densities.

The simulation we use for comparison is the “Millennium Simulation” carried out by the Virgo Consortium (Springel et al. 2005) coupled with the semi-analytic models presented by De Lucia et al. (2006). This simulation consisted of 2160^3 dark matter particles followed from $z = 127$ to the present day in a volume $500h^{-1}$ Mpc

on a side. The spatial resolution is $5h^{-1}$ Mpc, and the simulation is essentially complete for all galaxies with stellar mass greater than $3 \times 10^8 M_\odot$. This mass limit is comparable to the lowest mass galaxies in the ACSVCS. From this simulation, we selected a sample of low mass early-type cluster galaxies and their progenitors. We identified 126 massive galaxy clusters using the same criteria as in De Lucia et al. (2007), requiring a halo mass greater than $7 \times 10^{14} M_\odot$ at $z = 0$. This mass limit also corresponds roughly to the mass of Virgo (Böhringer et al. 1994). Within each of these clusters, we then selected all galaxies with $M_{z,sdss} > -19$ that have early-type morphologies, matching the low luminosity sample we have in the ACSVCS. Early-type galaxies were defined by the bulge-to-total luminosity ratio with $\Delta M < 1.56$ ($\Delta M = M_{bulge} - M_{total}$), using the empirical criteria of Simien & de Vaucouleurs (1986). In addition, we selected only galaxies with $g_{sdss} - z_{sdss} > 0.5$ at $z = 0$ in order to best match the colors of the ACSVCS galaxies. In total, we selected 15,506 simulated galaxies at $z = 0$ and all of their progenitors over 63 snapshots back to $z \sim 12$.

In Figure 18, we show the mass-weighted age of the stellar populations in the selected early-type dwarfs as a function of distance from the center of the cluster’s dark matter halo. The error bars show the 1σ width of the age distribution in each bin of radius. This figure clearly shows that the stellar age of the simulated dwarfs have a strong dependence on clustercentric radius, at least within a distance of 1.5 Mpc, with the central dwarfs having mean ages of 11.5 Gyr decreasing to 9 Gyr at the cluster outskirts. The radius within which the age gradient is evident is also the radius in Virgo within which we see elevated GC fractions.

The central dwarfs in the simulation may be older, but they also need to form their stars more intensely (higher peak star formation rates and densities) in order to have more of their stars in massive clusters. Figure 19a shows the average normalized star formation rate of early-type cluster dwarfs as a function of lookback time. The star formation rate is normalized to the final stellar mass of the galaxy. The two curves represent SFR histories for dwarfs divided into two bins of clustercentric radius at 1 Mpc from the cluster center. We note that these are average star formation histories, and that for any individual galaxy, the bursts of star formation are more intense, brief, and stochastic. Combining galaxies allows us to see that the central dwarfs have a more peaked SFR at earlier times with a rapid falloff, whereas the outer dwarfs not only have a lower peak but also more star formation extending to later times.

It has been suggested that massive star clusters form preferentially in high-pressure environments (Harris & Pudritz 1994; Elmegreen & Efremov 1997; Ashman & Zepf 2001), of which SFR surface density is one possible indication. Figure 19b shows the ratio of SFR surface density in central dwarfs to that in outer dwarfs. We calculate the SFR surface density using the SFR and the disk radius, which the semi-analytic models calculate using the analytic model of Mo, Mao & White (1998). Not only is the peak star formation rate higher in central dwarfs, but the *intensity* of star formation, as measured by the SFR surface density, is also higher during the epoch when these galaxies are forming most of their stars. At later times, the SFR surface density in the outer

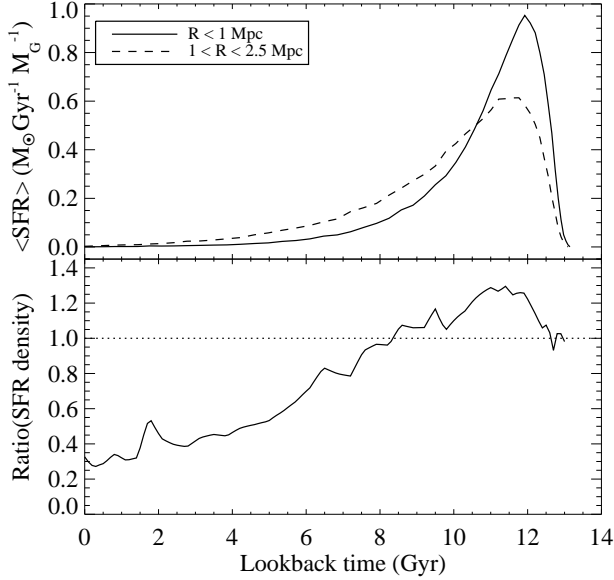


FIG. 19.— (a, top) Average normalized star formation rate versus lookback time for low mass early-type cluster galaxies in the Millennium simulation. The solid line shows the average SFR history for “central” galaxies within 1 Mpc of the cluster center, and the dashed line shows “outer” galaxies. Low mass early-type galaxies in the inner cluster regions formed their stars earlier and with higher peak star formation rate (SFR) than those in the outskirts. Higher peak SFRs could result in higher globular cluster mass fractions. (b, bottom) Average ratio in SFR surface density between inner and outer low mass early-type cluster galaxies as a function of lookback time. Galaxies in the inner regions have a higher SFR surface density during the period of highest total star formation ($t_{\text{lookback}} > 8$ Gyr). This results in central galaxies having a higher mass fraction in massive star clusters.

dwarfs is higher on average than that in central dwarfs, but this is at much lower absolute star formation rates and SFR surface densities. If GCs are formed in the same events that produced the bulk of these low mass galaxies, then we would expect that the central dwarfs would retain a higher fraction of their stellar mass in massive star clusters.

5.2.2. Inferring Cluster Formation Histories

We can quantify these effects more directly by inferring the cluster formation rate (CFR) history, using an empirical relationship between $S_{\mathcal{M}}$, the fraction of stellar mass formed in massive star clusters, and the SFR surface density, Σ_{SFR} . Fitting the data of Larsen & Richtler (2000), we adopt $S_{\mathcal{M}} \propto (\Sigma_{\text{SFR}})^{0.8}$, up to a maximum efficiency of 100%. The cluster formation rate then scales with a combination of the SFR and the SFR surface density as $\text{CFR} \propto \text{SFR} \times (\Sigma_{\text{SFR}})^{0.8}$. The Larsen & Richtler (2000) data measured the fraction of luminosity in young massive clusters (YMCs), which had ages between 10 and 500 Myr and more massive than $\sim 3 \times 10^4 M_{\odot}$. Given that most clusters will be destroyed over a Hubble time, we need to estimate what fraction of these clusters will survive. We adopt the two-stage disruption law of Whitmore, Chandar & Fall (2007) where “infant mortality” causes clusters to disrupt in constant numbers, $dN/d\tau \propto \tau^{-1}$, for ages less than a few $\times 10^8$ Gyr (Fall, Chandar & Whitmore 2005), and a constant mass loss over a Hubble time of $\mu_{\text{ev}} = 1.9 \times 10^4 M_{\odot} \text{Gyr}^{-1}$ due to two-body relaxation (Fall & Zhang 2001; Jordán

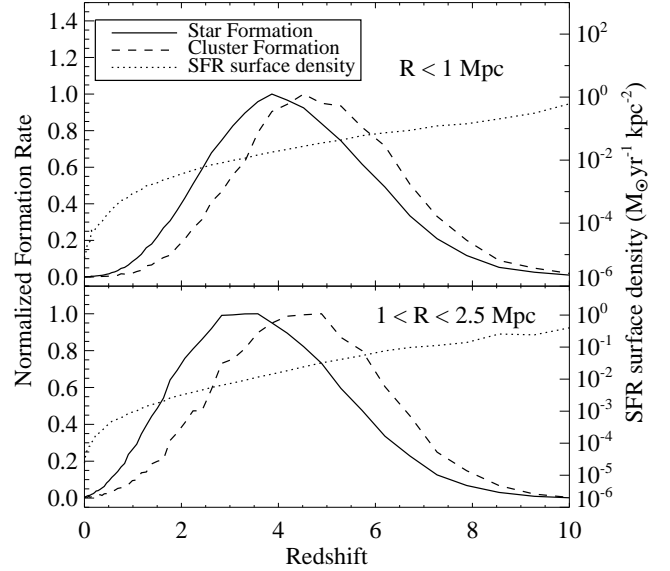


FIG. 20.— For central (top) and outer (bottom) early-type dwarfs in the Millennium Simulation, a comparison of the average star formation rate (solid), the average star formation rate surface density (dotted), and the inferred average cluster formation rate (dashed). The highest SFR surface densities occur at earlier times than the highest SFRs because the disks within which stars form are smaller at high redshift. If massive star clusters preferentially form at high SFR surface densities, then GCs in early-type dwarfs will, on average, have older ages and lower metallicities than the field stars. Formation rates are normalized to their maximum values.

et al. 2007). Starting with the data of Larsen & Richtler (2000), we estimate that $\sim 1.8\%$ of their young massive clusters survive to the present day. Using this formalism, we produce the corresponding cluster formation rate for central early-type dwarfs, normalized to the final mass in GCs.

Figure 20 compares the average SFR and SFR surface density as a function of redshift for the sample of central dwarfs (top) and outer dwarfs (bottom). While the SFR peaks at $z = 3.5 - 4$, Σ_{SFR} is highest at $z = 10$ and falls a factor of 35 by $z = 4$. Because the formation rate of massive star clusters depends on both quantities, their peak epoch of formation will be *earlier* than that of the stars. The result is that the CFR peaks at earlier redshift, $z \sim 4.5$ to 5, than the total star formation rate, a difference of ~ 350 –500 Myr. In all dwarfs, the dependence of massive star cluster formation on the SFR surface density naturally produces GCs that are older and more metal-poor than the stars.

Depending on how massive star cluster formation scales with SFR and SFR density, we also expect that the mean age difference between the GCs and the field would be different in the central and outer dwarfs. Because GCs in these dwarfs will mostly form at or before the SFR peak, they will always be old, but the field stars can continue to form at later times. This is evident when comparing the difference in lookback time for the SFR peaks for the central and outer simulated dwarfs in Figure 19a and the difference in their mean ages in Figure 18. The outer dwarfs have mass-weighted mean ages that are younger by ~ 2.5 Gyr, but the times of their peak star formation rates differ by only 0.1 Gyr. Figure 20 shows how the CFR peak happens at similar redshifts for all

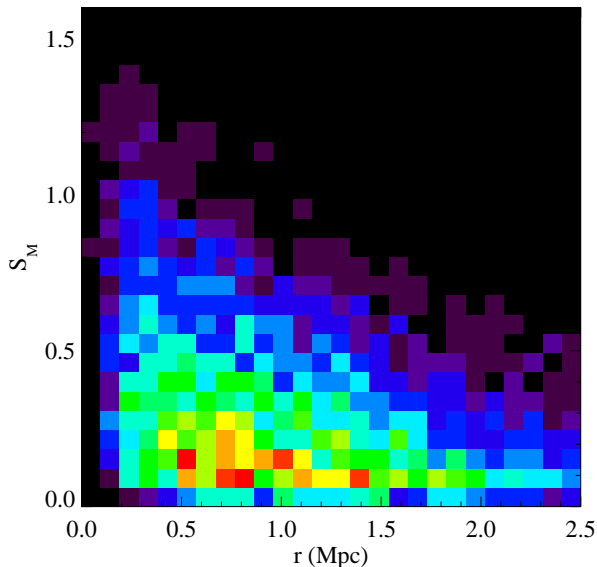


FIG. 21.— Simulated S_M versus clustercentric radius for early-type dwarfs in the Millennium simulation. Colors from purple to red (or black to white) symbolize lower to higher numbers of simulated dwarfs in a particular cell in this diagram. Like in the observations (Figures 10 and 11), there is a tendency for dwarf galaxies with higher S_M to be at the center of the cluster.

dwarfs, but the peak in star formation happens later in outer dwarfs. One prediction is then that, on average, the difference between the mean age of the metal-poor GCs and the mean age of the stars should be larger in dwarf galaxies with lower GC mass fractions (i.e., the mean age of the galaxy is proportional to S_M).

Lastly, we test whether this framework can produce higher GC mass fraction in the central dwarfs. Figure 21 shows S_M against clustercentric radius for simulated dwarfs. The absolute scale for S_M is highly sensitive to the assumed destruction but is not important for our purposes. It is the relative comparison between central and outer simulated dwarfs that is of interest, and the high- S_M simulated dwarfs do appear preferentially in the central regions, similar to what the data shows in Figures 10 and 11.

The simulations do not match the data exactly, as there also appears to be many low- S_M dEs within 1 Mpc, and the metallicities of the GCs as derived from the simulation are generally too high, but it is encouraging that this simple scaling for cluster formation in the Millennium Simulation can reproduce many of the observed trends. A more detailed treatment of ram pressure and tidal stripping in cluster cores in a higher resolution simulation may help resolve some discrepancies.

5.3. Possible Mechanisms for Quenching Star Formation

The central dwarfs may produce a higher fraction of GCs at or before their peak SFR, but it is also important that their subsequent star formation is rapidly quenched or kept at a low level. At these and lower masses, photoionization heating of the ISM by the UV background is believed to be an important mechanism for suppressing star formation in dwarf galaxies (Bullock, Kravtsov & Weinberg 2000; Benson et al. 2002), and this could

universally truncate the epoch of efficient formation of metal-poor GCs, although detailed work still needs to be done to show that reionization is a plausible mechanism for halting GC formation. At least one scenario (Cen 2001) has reionization as the cause for GC formation, another suggests that starburst-driven shocks may trigger GC formation (Scannapieco, Weisheit & Harlow 2004), and yet another shows that GCs themselves could plausibly be the source of reionizing photons (Ricotti 2004). So, the relationship between GC formation and reionization, if any, is still very much undetermined.

One potential problem with the scenario where reionization halts GC formation is that in the simulations of Bekki et al. (2006), the bias introduced by the truncation redshift is not very strong. Changing the truncation redshift from $z = 15$ to $z = 6$, for example, does not alter the S_N of galaxies by very much, and at least in these simulations, reionization-induced biased GC formation by itself does not seem to be able to explain the scatter in S_N for dEs. However, it may be sufficient to explain the general trend towards higher GC fractions at lower masses seen in Figure 17.

Another plausible explanation is that the environment plays an important role in quenching the later, lower level star formation that builds up the field. Ram pressure stripping of gas will be more efficient in low mass galaxies at the center of the cluster. Since these halos are the earliest to fall into the cluster, they will have their star formation quenched earlier and more efficiently than their counterparts in the outer cluster regions. Moore, Lake and Katz (1998) also showed through numerical simulations that “galaxy harassment” in clusters is efficient at transforming small spirals into low mass spheroidal galaxies. More recently, Mayer et al. (2007) used hydrodynamic simulations to demonstrate that the environmental effects of tidal shocks and ram pressure stripping can combine to create the most dark matter-dominated dwarf spheroidals (dSphs) in the Local Group. Although the Virgo dEs are much more massive than dSphs such as Draco or Ursa Minor, it is possible that similar processes caused them to fail in their conversion of gas to field stars. Ram pressure stripping in Virgo has been observed out to a cluster radius of 0.8 Mpc (Kenney, van Gorkom & Vollmer 2004), similar to the radius within which we see enhanced GC fractions. The comparison of central dEs and those on the outskirts, however, shows no strong differences between their observed properties. If harassment was important, we might expect different morphologies or surface brightness profiles (Sérsic n or r_e) in the two groups, but this is not the case. The cumulative GC color distributions of these two populations of dEs are also indistinguishable. If the central dEs were once much more luminous, we would expect them to be outliers on the color-magnitude relation, but the ones with high S_N are not. Only the innermost galaxies that are well within the M87 GC system and have no GCs are outliers and are red for their luminosities. These galaxies are good candidates for having been harassed.

5.4. Globular Cluster Destruction

Up until now, we have only discussed the possible variation in formation histories to explain the observed trends in GC fraction. However, star clusters can also be destroyed, and we expect that a substantial fraction of

clusters initially formed will not survive a Hubble time. Observations of young star clusters in nearby galaxies show that most star clusters are disrupted very early (Fall et al. 2005; Bastian et al. 2005). In addition, subsequent evolution through two-body relaxation, stellar mass loss, and tidal shocks will destroy even more low mass clusters (Fall & Rees 1977; Vesperini 1998; Fall & Zhang 2001). Globular clusters are thus the survivors of what was once a much larger population of star clusters. Any differences in the survival rates between different galaxies could produce different GC fractions in the present day.

Unfortunately, the cosmological simulations used to study galaxy formation cannot at the present time model GC destruction. One benefit of studying trends in terms of S_M , or GC mass fraction, is that while most of the destroyed star clusters after the initial 1 Gyr are preferentially low mass, most of the mass remains in the higher mass objects. Thus, GC mass fraction is more robust against disruption processes that preferentially destroy low mass clusters. If, however, there was a mechanism that could affect the survival efficiency of massive clusters—perhaps variable infant mortality or dynamical friction as influenced by the dark matter halo profile—then destruction could play a role in driving the trends in GC mass fraction. This mechanism would require central dwarfs to be able to retain a larger fraction of the massive star clusters than their counterparts at larger cluster radii. This is perhaps counter to what one might expect if the cluster tidal field had a role in stripping or destroying GCs. We also see no signs in our data that central dwarfs have higher mean GC masses or different GC luminosity functions, things that might point to internal destruction being a dominant mechanism driving GC fractions.

For a real test of the mechanisms that drive GC formation efficiency, it would be extremely beneficial to have more and better simulations of galaxies and their star cluster populations. Both hydrodynamic simulations and dark matter simulations coupled with semi-analytic models can provide useful quantitative predictions. These would ideally be able to produce a $z = 0$ volume comparable to the Virgo cluster with a stellar mass resolution that would allow the resolution of GC mass objects ($\sim 10^5 M_\odot$).

5.5. S_N Variation in Metal-poor and Metal-rich GCs

Another result of this study is the behavior of the specific frequencies of blue and red GCs. The variation in S_N is dominated by the blue, metal-poor GCs, although the red GCs do exhibit similar trends with fewer GCs and lower significance. Figure 8 shows that the fraction of red GCs rarely exceeds 50% and that the trend of increasing red fraction with galaxy mass either flattens or turns over for the most massive galaxies. This suggests that massive ellipticals have accreted the most dwarf-like galaxies, the presumed original hosts of metal-poor GCs, or that the dwarfs which they accreted had the highest S_N , or both. Also, the rise in red GC fraction from $M_z = -19$ to $M_z = -22$ requires that $S_{N,z,blue}$ and $S_{N,z,red}$ respectively fall and rise in equal proportions to produce the nearly constant $S_{N,z}$ over this range. The fraction of blue GCs is lowest where the total $S_{N,z}$ is at a minimum, implying again that they are driving the

overall trends.

The higher values of $S_{N,z,red}$ for the massive galaxies, in particular M87, means that the formation of metal-rich GCs also occurs at different efficiencies. For massive galaxies, these results are consistent with the data of Rhode et al. (2005), who found that the mass-normalized number of GCs, T_{red} , is positively correlated with galaxy mass (shown in Figure 4 of Brodie & Strader 2006). Could these metal-rich GCs have been accreted from dwarfs in a scenario similar to that described for the metal-poor GCs? Figure 15 shows that the number fraction of red GCs may also be enhanced in central dwarfs, like the metal-poor GCs, but it is unclear whether a biasing scenario similar to the one described above provide an explanation since we would expect that the formation of metal-rich GCs at a later time might actually be suppressed. However, the numbers we observe are very small and uncertain and may be sensitive to the dividing color between blue and red GCs, which is chosen to be the same in all galaxies at these luminosities. Another possibility is that the trend in the red GCs is determined more by the mass of the host, with red GCs forming in the most massive progenitor, and the more massive protogalaxies forming their stars earlier and with higher star formation rates. This is consistent with observations of the stellar populations of elliptical galaxies, which find that the stars in massive ellipticals ($L > L^*$) form have old ages and high $[\alpha/Fe]$ —i.e., they formed early and rapidly—while lower mass early-type galaxies have younger mean ages and lower $[\alpha/Fe]$ (Thomas et al. 2005). Similar trends in $[\alpha/Fe]$ are seen in the GCs of these galaxies (Puzia et al. 2006).

The fact that we see the same trends for both the blue and red GC sub-populations suggests the possibility that the two populations are not very distinct, and that their separation is merely the result of placing a dividing line on a continuum of GC properties. This possibility has been raised by Yoon, Yi, & Lee (2006), who suggest that the GC metallicity bimodality in early-type galaxies is a result of a nonlinear metallicity-color relation. Although our data does not constrain this hypothesis, we do not observe a clear distinction between blue and red GC fractions across galaxy mass or environment.

6. CONCLUSIONS

We have measured globular cluster specific frequencies (S_N), luminosity fractions (S_L), and stellar mass fractions (S_M) for 100 early-type galaxies in the ACS Virgo Cluster Survey. These galaxies span the mass range from giants to dwarfs ($-22 < M_B < -15$) and these represent the largest homogeneous catalog of GC number and mass fractions to date. We have studied these quantities as a function of galaxy mass and environment and find that:

1. Globular cluster fractions can be high ($S_{N,z} > 2$) for both high and low luminosity early-type galaxies, but are universally low for intermediate luminosity galaxies ($-22 < M_z < -19$).
2. There is a large spread in GC fraction in early-type dwarfs ($0 < S_{N,z} < 5.5$) which can be understood as an underlying dependence on environment. Almost all dwarfs ($M_z > -19$) with $S_{N,z} > 2$ are within a projected radius of 1 Mpc from M87 and the cluster center (or 1.5 Mpc in three-dimensional

cluster radius). The spatial distributions of GCs in the high- S_N dwarfs are centrally concentrated, showing that they are intrinsic to the host dwarf and not interloping GCs from M87 or an intra-cluster population. We do not detect higher GC fractions in dwarfs around the other massive ellipticals in the cluster. We present this as evidence that GC formation in low mass galaxies is biased towards the densest environments.

3. Galaxies within $R_p \sim 40$ kpc of M87 and M49 have few or no GCs, and are likely to have had their GC systems tidally stripped by their giant neighbors. Galaxies out to $R_p \sim 100$ kpc from M87 (VCC 1185) also appear to be affected.
4. Analyzing the blue and red GC populations separately, we find that the fraction of red GCs increases with galaxy luminosity until $M_z \sim -22$ at which point it flattens or declines. Trends in GC fraction are dominated by the blue GCs, although the $S_{N,z}$ of red GCs does exhibit similar relative enhancement for massive galaxies, and possibly shows a weak enhancement for central dwarfs.
5. We use a globally averaged $\mathcal{M}_h/\mathcal{M}_{G\star}-\mathcal{M}_{G\star}$ relation from halo occupation studies to test whether trends in GC fraction can be explained by the assumption that the mass in GCs is directly proportional to the halo mass, $\mathcal{M}_{GC} \propto \mathcal{M}_h$. While this may be able to explain the mean trend in $S_{\mathcal{M}}$, it is unable to account simultaneously for all dwarfs, particularly the dwarfs with high GC fractions in the cluster's central regions.
6. Comparisons with semi-analytic models of galaxy formation in the Millennium Simulation show that early-type dwarfs in the central 1 Mpc of massive galaxy clusters are expected to be older and have higher peak star formation rates and SFR surface densities than their counterparts on the outskirts of the cluster. The higher stellar mass fractions in globular cluster for central dwarfs can be explained if higher SFR surface densities are responsible for more efficient formation of massive star clusters.
7. The peak SFR surface density in simulated dwarfs occurs before the peak SFR, which we propose as an explanation for why GCs are, on average, both older and more metal-poor than the field stars in their host galaxies.

We present a picture of globular cluster system formation in the Virgo Cluster where the highest GC mass fractions are formed in the oldest systems. These progenitors formed a larger fraction of their stars at higher peak SFR surface densities, and also have star formation suppressed at later times. In regions of high density, halos collapse and star formation starts earlier, and the mechanisms for truncating and suppressing subsequent star formation are stronger. For all dwarfs, the highest SFR surface densities occur earlier than the peak SFR, naturally producing the metal-poor GC populations we see today—old (> 10 Gyr) and more metal-poor than the bulk of the field stars. Merging of many low mass progenitors with high GC fractions produce the extremely high

S_N for blue GCs seen in the cD galaxy, M87. They may also, at a lower level, produce the elevated blue GC fractions seen in other massive ellipticals. Future detailed simulations of GC system formation will be crucial to test, in a quantitative way, the scenarios of galaxy and GC system formation that we are beginning to assemble.

E. W. P. gratefully acknowledges the support of the National Research Council of Canada's Plaskett Research Fellowship at the Herzberg Institute of Astrophysics. We thank Gabriella De Lucia, Gerard Lemson, and Darren Croton for their help with the Millennium Simulation, and thank Rupali Chandar, Dean McLaughlin, Anil Seth, and Peter Stetson for useful discussions and comments on the manuscript. We also thank Peter Stetson for providing point spread functions used in the analysis of our WFPC2 data. We thank Naoyuki Tamura, who provided the numbers for their M87 GC radial profile. We are grateful to the anonymous referee who provided comments that improved the manuscript. M. J. W. and M. T. acknowledge support through NSF grant AST 02-05960.

This publication makes use of data products from the Sloan Digital Sky Survey (SDSS). Funding for SDSS and SDSS-II has been provided by the Alfred P. Sloan Foundation, the Participating Institutions, the National Science Foundation, the U.S. Department of Energy, the National Aeronautics and Space Administration, the Japanese Monbukagakusho, the Max Planck Society, and the Higher Education Funding Council for England. The SDSS Web site is <http://www.sdss.org/>.

The SDSS is managed by the Astrophysical Research Consortium (ARC) for the Participating Institutions. The Participating Institutions are the American Museum of Natural History, Astrophysical Institute Potsdam, University of Basel, University of Cambridge, Case Western Reserve University, The University of Chicago, Drexel University, Fermilab, the Institute for Advanced Study, the Japan Participation Group, The Johns Hopkins University, the Joint Institute for Nuclear Astrophysics, the Kavli Institute for Particle Astrophysics and Cosmology, the Korean Scientist Group, the Chinese Academy of Sciences (LAMOST), Los Alamos National Laboratory, the Max-Planck-Institute for Astronomy (MPIA), the Max-Planck-Institute for Astrophysics (MPA), New Mexico State University, Ohio State University, University of Pittsburgh, University of Portsmouth, Princeton University, the United States Naval Observatory, and the University of Washington.

This publication makes use of data products from the Two Micron All Sky Survey, which is a joint project of the University of Massachusetts and the Infrared Processing and Analysis Center/California Institute of Technology, funded by the National Aeronautics and Space Administration and the National Science Foundation.

This research has made use of the NASA/IPAC Extragalactic Database (NED) which is operated by the Jet Propulsion Laboratory, California Institute of Technology, under contract with the National Aeronautics and Space Administration.

Facilities: HST(ACS,WFPC2)

REFERENCES

- Adelman-McCarthy, J. K., et al. 2007, *ApJS*, 172, 634
- Ashman, K. M., & Zepf, S. E. 1992, *ApJ*, 384, 50
- Ashman, K. M., & Zepf, S. E. 1998, *Globular cluster systems / Keith M. Ashman, Stephen E. Zepf. Cambridge, U. K. ; New York : Cambridge University Press, 1998. (Cambridge astrophysics series ; 30) QB853.5 .A84 1998*
- Ashman, K. M., & Zepf, S. E. 2001, *AJ*, 122, 1888
- Bagget, S. et al. 2002, in *HST WFPC2 Data Handbook*, v. 4.0, ed. B. Mobasher, Baltimore, STScI
- Bastian, N., Gieles, M., Lamers, H. J. G. L. M., Scheepmaker, R. A., & de Grijs, R. 2005, *A&A*, 431, 905
- Beasley, M. A., Baugh, C. M., Forbes, D. A., Sharples, R. M., & Frenk, C. S. 2002, *MNRAS*, 333, 383
- Bekki, K., Yahagi, H., & Forbes, D. A. 2006, *ApJ*, 645, L29
- Benson, A. J., Frenk, C. S., Lacey, C. G., Baugh, C. M., & Cole, S. 2002, *MNRAS*, 333, 177
- Berlind, A. A., & Weinberg, D. H. 2002, *ApJ*, 575, 587
- Bertin, E., & Arnouts, S. 1996, *A&AS*, 117, 393
- Binggeli, B., Sandage, A., & Tammann, G. A. 1985, *AJ*, 90, 1681
- Blakeslee, J. P. 1997, *ApJ*, 481, L59
- Blakeslee, J. P., Tonry, J. L., & Metzger, M. R. 1997, *AJ*, 114, 482
- Blakeslee, J. P. 1999, *AJ*, 118, 1506
- Blakeslee, J. P., Meurer, G. R., Ford, H. C., Benitez, N., White, R. L., Zekser, K. C., & Sirianni, M. 2003, *Extragalactic Globular Clusters and their Host Galaxies*, 25th meeting of the IAU, Joint Discussion 6, 17 July 2003, Sydney, Australia, 6
- Blakeslee, J. P., Anderson, K. R., Meurer, G. R., Benítez, N., & Magee, D. 2003, *Astronomical Data Analysis Software and Systems XII*, 295, 257
- Blanton, M. R., & Roweis, S. 2007, *AJ*, 133, 734
- Bohringer, H., Briel, U. G., Schwarz, R. A., Voges, W., Hartner, G., & Trumper, J. 1994, *Nature*, 368, 828
- Brodie, J. P., & Huchra, J. P. 1991, *ApJ*, 379, 157
- Brodie, J. P., & Strader, J. 2006, *ARA&A*, 44, 193
- Bullock, J. S., Kravtsov, A. V., & Weinberg, D. H. 2000, *ApJ*, 539, 517
- Cantiello, M., & Blakeslee, J. P. 2007, *ApJ*, 669, 982
- Cen, R. 2001, *ApJ*, 560, 592
- Cappellari, M., et al. 2006, *MNRAS*, 366, 1126
- Chaboyer, B., Demarque, P., Kernan, P. J., & Krauss, L. M. 1996, *Science*, 271, 957
- Chabrier, G. 2003, *PASP*, 115, 763
- Chandar, R., Whitmore, B., & Lee, M. G. 2004, *ApJ*, 611, 220
- Côté, P., Marzke, R. O., & West, M. J. 1998, *ApJ*, 501, 554
- Côté, P., Marzke, R. O., West, M. J., & Minniti, D. 2000, *ApJ*, 533, 869
- Côté, P., et al. 2001, *ApJ*, 559, 828
- Côté, P., McLaughlin, D. E., Cohen, J. G., & Blakeslee, J. P. 2003, *ApJ*, 591, 850
- Côté, P., et al. 2004, *ApJS*, 153, 223 (Paper I)
- Côté, P., et al. 2006, *ApJS*, 165, 57
- Croton, D. J., et al. 2006, *MNRAS*, 365, 11
- Côté, P., et al. 2007, *ApJ*, submitted
- De Lucia, G., Springel, V., White, S. D. M., Croton, D., & Kauffmann, G. 2006, *MNRAS*, 366, 499
- De Lucia, G., & Blaizot, J. 2007, *MNRAS*, 375, 2
- de Vaucouleurs, G., de Vaucouleurs, A., Corwin, H. G., Jr., Buta, R. J., Paturel, G., & Fouque, P. 1991, *Volume 1-3, XII*, 2069 pp. 7 figs.. Springer-Verlag Berlin Heidelberg New York
- Dekel, A., & Birnboim, Y. 2006, *MNRAS*, 368, 2
- Diemand, J., Madau, P., & Moore, B. 2005, *MNRAS*, 364, 367
- Dirsch, B., Richtler, T., Geisler, D., Forte, J. C., Bassino, L. P., & Gieren, W. P. 2003a, *AJ*, 125, 1908
- Dirsch, B., Richtler, T., & Bassino, L. P. 2003b, *A&A*, 408, 929
- Dirsch, B., Schuberth, Y., & Richtler, T. 2005, *A&A*, 433, 43
- Durrell, P. R., Harris, W. E., Geisler, D., & Pudritz, R. E. 1996a, *AJ*, 112, 972
- Durrell, P. R., McLaughlin, D. E., Harris, W. E., & Hanes, D. A. 1996b, *ApJ*, 463, 543
- Elmegreen, B. G., & Efremov, Y. N. 1997, *ApJ*, 480, 235
- Fall, S. M., & Rees, M. J. 1977, *MNRAS*, 181, 37P
- Fall, S. M., & Zhang, Q. 2001, *ApJ*, 561, 751
- Fall, S. M., Chandar, R., & Whitmore, B. C. 2005, *ApJ*, 631, L133
- Ferrarese, L., et al. 2006a, *ApJS*, 164, 334
- Ferrarese, L., et al. 2006b, *ApJ*, 644, L21
- Forbes, D. A., Brodie, J. P., & Huchra, J. 1996, *AJ*, 112, 2448
- Forbes, D. A. 2005, *ApJ*, 635, L137
- Ford, H. C., et al. 1998, *Proc. SPIE*, 3356, 234
- Freedman, W. L., et al. 2001, *ApJ*, 553, 47
- Gao, L., Springel, V., & White, S. D. M. 2005, *MNRAS*, 363, L66
- Geha, M., Guhathakurta, P., & van der Marel, R. P. 2003, *AJ*, 126, 1794
- Goudfrooij, P., Strader, J., Brennenman, L., Kissler-Patig, M., Minniti, D., & Edwin Huizinga, J. 2003, *MNRAS*, 343, 665
- Gómez, M., & Richtler, T. 2004, *A&A*, 415, 499
- Hasegan, M., et al. 2005, *ApJ*, 627, 203 (Paper VII)
- Harris, G. L. H., Harris, W. E., & Geisler, D. 2004, *AJ*, 128, 723
- Harris, W. E., & van den Bergh, S. 1981, *AJ*, 86, 1627
- Harris, W. E. 1991, *ARA&A*, 29, 543
- Harris, W. E., & Pudritz, R. E. 1994, *ApJ*, 429, 177
- Harris, W. E., Harris, G. L. H., & McLaughlin, D. E. 1998, *AJ*, 115, 1801
- Harris, W. E., & Harris, G. L. H. 2002, *AJ*, 123, 3108
- Hoekstra, H., Hsieh, B. C., Yee, H. K. C., Lin, H., & Gladders, M. D. 2005, *ApJ*, 635, 73
- Jarrett, T. H., Chester, T., Cutri, R., Schneider, S. E., & Huchra, J. P. 2003, *AJ*, 125, 525
- Jordán, A., West, M. J., Côté, P., & Marzke, R. O. 2003, *AJ*, 125, 1642
- Jordán, A., Côté, P., West, M. J., Marzke, R. O., Minniti, D., & Rejkuba, M. 2004a, *AJ*, 127, 24
- Jordán, A., et al. 2004a, *ApJS*, 154, 509 (Paper II)
- Jordán, A., et al. 2004b, *ApJ*, 613, 279 (Paper III)
- Jordán, A., et al. 2005, *ApJ*, 634, 1002 (Paper X)
- Jordán, A., et al. 2006, *ApJ*, 651, L25
- Jordán, A., et al. 2007, *ApJS*, 171, 101 (Paper XII)
- Kauffmann, G., et al. 2003, *MNRAS*, 341, 54
- Kenney, J. D. P., van Gorkom, J. H., & Vollmer, B. 2004, *AJ*, 127, 3361
- King, I. R. 1966, *AJ*, 71, 64
- Kodama, T., Arimoto, N., Barger, A. J., & Arag'ón-Salamanca, A. 1998, *A&A*, 334, 99
- Koekemoer, A. M., Fruchter, A. S., Hook, R. N., & Hack, W. 2002, *The 2002 HST Calibration Workshop : Hubble after the Installation of the ACS and the NICMOS Cooling System*, Proceedings of a Workshop held at the Space Telescope Science Institute, Baltimore, Maryland, October 17 and 18, 2002. Edited by Santiago Arribas, Anton Koekemoer, and Brad Whitmore. Baltimore, MD: Space Telescope Science Institute, 2002., p.339, 339
- Kundu, A., & Whitmore, B. C. 2001a, *AJ*, 121, 2950
- Kundu, A., & Whitmore, B. C. 2001b, *AJ*, 122, 1251
- Kravtsov, A. V., & Gnedin, O. Y. 2005, *ApJ*, 623, 650
- Kronawitter, A., Saglia, R. P., Gerhard, O., & Bender, R. 2000, *A&AS*, 144, 53
- Larsen, S. S., & Richtler, T. 2000, *A&A*, 354, 836
- Larsen, S. S., Brodie, J. P., Huchra, J. P., Forbes, D. A., & Grillmair, C. J. 2001, *AJ*, 121, 2974
- Lotz, J. M., Miller, B. W., & Ferguson, H. C. 2004, *ApJ*, 613, 262
- Mandelbaum, R., Seljak, U., Kauffmann, G., Hirata, C. M., & Brinkmann, J. 2006, *MNRAS*, 368, 715
- Mayer, L., Kazantzidis, S., Mastrogiuseppe, C., & Wadsley, J. 2007, *Nature*, 445, 738
- McLaughlin, D. E. 1999a, *AJ*, 117, 2398
- McLaughlin, D. E. 1999b, *ApJ*, 512, L9
- Mei, S., et al. 2005a, *ApJS*, 156, 113
- Mei, S., et al. 2005b, *ApJ*, 625, 121 (Paper V)
- Mei, S., et al. 2007, *ApJ*, 655, 144
- Mieske, S., et al. 2006, *ApJ*, 653, 193 (Paper XIV)
- Miller, B. W., Lotz, J. M., Ferguson, H. C., Stiavelli, M., & Whitmore, B. C. 1998, *ApJ*, 508, L133
- Miller, B. W., & Lotz, J. M. 2007, *ApJ*, 670, 1074
- Mo, H. J., Mao, S., & White, S. D. M. 1998, *MNRAS*, 295, 319
- Moore, B., Lake, G., & Katz, N. 1998, *ApJ*, 495, 139
- Moore, B., Diemand, J., Madau, P., Zemp, M., & Stadel, J. 2006, *MNRAS*, 368, 563
- Napolitano, N. R., et al. 2005, *MNRAS*, 357, 691
- Peng, E. W., Ford, H. C., & Freeman, K. C. 2004, *ApJ*, 602, 685

- Peng, E. W., et al. 2006a, ApJ, 639, 95 (Paper IX)
Peng, E. W., et al. 2006b, ApJ, 639, 838 (Paper XI)
Puzia, T. H., Kissler-Patig, M., & Goudfrooij, P. 2006, ApJ, 648, 383
Puzia, T. H., & Sharina, M. E. 2007, ArXiv e-prints, 710, arXiv:0710.1550
Rhode, K. L., & Zepf, S. E. 2001, AJ, 121, 210
Rhode, K. L., & Zepf, S. E. 2004, AJ, 127, 302
Rhode, K. L., Zepf, S. E., & Santos, M. R. 2005, ApJ, 630, L21
Ricotti, M. 2004, The Formation and Evolution of Massive Young Star Clusters, 322, 509
Romanowsky, A. J., Douglas, N. G., Arnaboldi, M., Kuijken, K., Merrifield, M. R., Napolitano, N. R., Capaccioli, M., & Freeman, K. C. 2003, Science, 301, 1696
Salpeter, E. E. 1955, ApJ, 121, 161
Guzik, J., & Seljak, U. 2002, MNRAS, 335, 311
Santos, M. R. 2003, Extragalactic Globular Cluster Systems, 348
Schlegel, D. J., Finkbeiner, D. P., & Davis, M. 1998, ApJ, 500, 525
Searle, L., & Zinn, R. 1978, ApJ, 225, 357
Sersic, J. L. 1968, Cordoba, Argentina: Observatorio Astronomico, 1968
Seth, A., Olsen, K., Miller, B., Lotz, J., & Telford, R. 2004, AJ, 127, 798
Sirianni, M., Jee, M.J., Bentez, N., Blakeslee, J.P., Martel, A.R., Meurer, G., Clampin, M., De Marchi, G., Ford, H.C., Gilliland, R., Hartig, G.F., Illingworth, G.D., Mack, J., & McCann, W.J. 2005, PASP, accepted
Sivakoff, G. R., et al. 2007, ApJ, 660, 1246
Skrutskie, M. F., et al. 2006, AJ, 131, 1163
Spergel, D. N., et al. 2007, ApJS, 170, 377
Spitler, L. R., Forbes, D. A., Strader, J., Brodie, J. P., & Gallagher, J. S., III 2007, ArXiv e-prints, 712, arXiv:0712.1382
Springel, V., et al. 2005, Nature, 435, 629
Strader, J., Brodie, J. P., Spitler, L., & Beasley, M. A. 2006, AJ, 132, 2333
Thomas, D., Maraston, C., Bender, R., & Mendes de Oliveira, C. 2005, ApJ, 621, 673
Tonry, J. L., Dressler, A., Blakeslee, J. P., Ajhar, E. A., Fletcher, A. B., Luppino, G. A., Metzger, M. R., & Moore, C. B. 2001, ApJ, 546, 681
Tremonti, C. A., et al. 2004, ApJ, 613, 898
Vale, A., & Ostriker, J. P. 2007, ArXiv Astrophysics e-prints, arXiv:astro-ph/0701096
van den Bergh, S. 1975, ARA&A, 13, 217
van den Bosch, F. C., Yang, X., & Mo, H. J. 2003, MNRAS, 340, 771
van Dokkum, P. G. 2001, PASP, 113, 1420
Vesperini, E. 1998, MNRAS, 299, 1019
West, M. J. 1993, MNRAS, 265, 755
West, M. J., Cote, P., Jones, C., Forman, W., & Marzke, R. O. 1995, ApJ, 453, L77
West, M. J., Côté, P., Marzke, R. O., & Jordán, A. 2004, Nature, 427, 31
West, A. A., et al. 2007, AJ, submitted
Whitmore, B. C., Chandar, R., & Fall, S. M. 2007, AJ, 133, 1067
Williams, B. F., et al. 2007, ApJ, 654, 835
Yoon, S.-J., Yi, S. K., & Lee, Y.-W. 2006, Science, 311, 1129
Zepf, S. E., Ashman, K. M., & Geisler, D. 1995, ApJ, 443, 570

TABLE 1
 GLOBAL PROPERTIES OF ACS VIRGO CLUSTER SURVEY GALAXIES

No. (1)	VCC (2)	M_V (3)	M_Z (4)	R_p (5)	R_{3D} (6)	$L_{z,*}$ (7)	M_* (8)
1	1226	-22.90	-23.87	1.27	1.28 ± 0.39	263.04	531.84 ± 110.48
2	1316	-22.66	-23.86	0.00	0.00	188.40	302.27 ± 79.13
3	1978	-22.41	-23.42	0.94	1.04 ± 0.46	167.62	339.32 ± 50.28
4	881	-22.54	-23.53	0.36	1.49 ± 0.42	181.42	289.63 ± 59.87
5	798	-22.34	-23.25	1.71	2.09 ± 0.42	132.84	186.50 ± 43.84
6	763	-22.29	-23.20	0.43	2.09 ± 0.44	141.95	236.49 ± 61.04
7	731	-22.31	-23.37	1.53	6.76 ± 0.54	141.76	226.21 ± 52.45
8	1535	-21.38	-22.40	1.37	...	57.88	77.21 ± 16.21
9	1903	-21.18	-22.19	0.82	1.87 ± 0.35	50.26	83.87 ± 19.10
10	1632	-21.36	-22.33	0.34	0.63 ± 0.38	60.33	95.35 ± 16.89
11	1231	-20.70	-21.58	0.31	1.30 ± 0.36	32.37	53.46 ± 12.30
12	2095	-20.78	-20.95	1.59	...	33.74	52.75 ± 10.12
13	1154	-20.85	-21.79	0.47	0.66 ± 0.38	36.86	77.95 ± 13.64
14	1062	-20.56	-21.34	0.77	1.42 ± 0.36	28.65	52.69 ± 8.88
15	2092	-20.46	-21.64	1.54	1.61 ± 0.38	25.55	47.32 ± 7.66
16	369	-20.19	-20.41	0.79	1.04 ± 0.37	20.17	32.46 ± 7.67
17	759	-20.44	-21.41	0.46	0.60 ± 0.40	25.74	45.15 ± 10.04
18	1692	-20.26	-21.04	1.54	1.64 ± 0.40	21.85	33.97 ± 6.55
19	1030	-20.45	-21.38	0.30	0.33 ± 0.39	22.63	13.32 ± 9.05
20	2000	-19.60	-20.66	1.03	2.03 ± 0.35	11.71	23.76 ± 4.10
21	685	-20.11	-21.04	1.33	...	19.12	31.23 ± 6.69
22	1664	-19.90	-20.97	0.48	0.77 ± 0.38	15.39	26.00 ± 6.15
23	654	-19.88	-20.59	1.35	...	14.22	22.74 ± 4.12
24	944	-19.80	-20.66	0.86	1.05 ± 0.38	13.94	29.14 ± 4.88
25	1938	-19.93	-20.86	0.89	1.00 ± 0.40	15.71	24.86 ± 5.50
26	1279	-19.78	-20.72	0.04	0.47 ± 0.40	13.42	22.03 ± 4.03
27	1720	-19.63	-20.68	0.94	0.97 ± 0.38	11.55	20.21 ± 5.31
28	355	-19.42	-20.41	1.07	1.55 ± 0.36	10.06	15.78 ± 3.62
29	1619	-19.36	-20.19	0.33	1.51 ± 0.36	8.65	17.24 ± 3.12
30	1883	-19.68	-20.73	1.65	1.69 ± 0.38	11.19	16.66 ± 3.92
31	1242	-19.38	-20.29	0.49	1.42 ± 0.43	9.07	15.27 ± 3.17
32	784	-19.31	-20.26	1.00	1.30 ± 0.37	8.48	16.79 ± 3.14
33	1537	-18.99	-19.95	0.39	1.18 ± 0.36	6.18	10.24 ± 2.35
34	778	-19.56	-20.03	0.79	1.17 ± 0.41	10.73	18.18 ± 4.19
35	1321	-18.80	-19.93	1.26	1.99 ± 0.35	4.86	6.98 ± 1.75
36	828	-19.15	-20.07	0.38	1.42 ± 0.42	7.51	13.69 ± 3.00
37	1250	-18.98	-20.10	0.06	0.79 ± 0.57	5.23	3.68 ± 2.04
38	1630	-19.07	-20.06	0.34	0.51 ± 0.38	7.03	11.61 ± 2.39
39	1146	-18.93	-19.64	0.28	0.60 ± 0.38	5.71	8.69 ± 2.17
40	1025	-19.58	-20.57	1.24	5.98 ± 0.53	10.90	21.39 ± 4.25
41	1303	-18.84	-19.80	0.97	0.98 ± 0.39	5.55	10.39 ± 2.33
42	1913	-18.87	-19.74	1.58	1.67 ± 0.40	5.67	10.74 ± 2.72
43	1327	-19.10	-19.81	0.04	1.45 ± 0.51	8.36	17.24 ± 2.34
44	1125	-19.07	-19.44	0.24	...	6.80	8.06 ± 3.40
45	1475	-18.56	-19.42	1.13	1.15 ± 0.38	4.07	7.73 ± 1.50
46	1178	-18.35	-19.35	1.22	1.48 ± 0.37	3.64	7.09 ± 1.42
47	1283	-18.65	-19.70	0.34	0.86 ± 0.41	4.83	9.08 ± 1.79
48	1261	-18.42	-19.21	0.47	1.44 ± 0.51	3.14	4.87 ± 1.69
49	698	-18.78	-19.71	0.58	1.80 ± 0.43	5.03	9.52 ± 2.56
50	1422	-17.97	-18.73	0.62	1.60 ± 0.43	2.18	3.82 ± 1.35
51	2048	-17.85	-18.57	1.32	...	1.89	2.94 ± 1.08
52	1871	-17.31	-18.32	0.79	1.43 ± 0.44	1.36	2.26 ± 0.58
53	9	-18.04	-18.80	1.57	1.64 ± 0.65	2.17	3.08 ± 0.61
54	575	-18.42	-19.33	1.34	5.30 ± 0.61	3.56	5.00 ± 1.75
55	1910	-17.39	-18.33	0.82	1.11 ± 0.37	1.43	2.10 ± 0.81
56	1049	-16.69	-17.34	1.26	1.43 ± 0.53	0.60	0.52 ± 0.40
57	856	-17.57	-18.25	0.76	0.76 ± 0.47	1.47	2.22 ± 0.85
58	140	-17.51	-18.27	1.24	1.30 ± 0.46	1.37	2.33 ± 0.71
59	1355	-17.51	-18.16	0.50	0.52 ± 0.63	1.29	1.82 ± 0.35
60	1087	-17.79	-18.64	0.25	0.34 ± 0.46	1.84	3.29 ± 1.07
61	1297	-17.67	-18.75	0.04	0.23 ± 0.46	1.95	3.96 ± 0.62
62	1861	-17.60	-18.34	0.80	1.15 ± 0.45	1.63	2.88 ± 1.00
63	543	-17.41	-18.19	0.91	1.44 ± 0.44	1.27	2.19 ± 0.65
64	1431	-17.39	-18.25	0.34	0.90 ± 0.45	1.37	2.20 ± 0.74
65	1528	-17.16	-18.04	0.34	0.70 ± 0.45	1.06	1.63 ± 0.48
66	1695	-17.49	-18.32	0.43	0.46 ± 0.54	1.30	1.69 ± 0.78
67	1833	-17.13	-17.89	1.22	1.33 ± 0.45	0.97	0.86 ± 0.48
68	437	-17.82	-18.69	1.62	1.65 ± 0.48	1.92	2.80 ± 1.25
69	2019	-17.36	-18.18	1.08	1.13 ± 0.48	1.17	1.02 ± 0.72
70	33	-16.39	-17.01	1.48	2.19 ± 0.57	0.46	0.43 ± 0.25
71	200	-17.12	-17.80	1.02	1.70 ± 0.59	0.95	1.34 ± 0.49
72	571	-17.32	-18.29	1.40	7.27 ± 1.01	1.07	0.98 ± 0.65
73	21	-16.83	-17.38	1.58	...	0.58	0.56 ± 0.37
74	1488	-16.78	-17.34	0.88	...	0.57	0.41 ± 0.38
75	1779	-16.90	-17.38	0.89	...	0.63	1.02 ± 0.38

TABLE 1 — *Continued*

No. (1)	VCC (2)	M_V (3)	M_z (4)	R_p (5)	R_{3D} (6)	$L_{z,*}$ (7)	M_* (8)
76	1895	-16.60	-17.29	1.16	1.47 ± 0.37	0.57	0.76 ± 0.39
77	1499	-16.53	-16.95	0.22	...	0.34	0.14 ± 0.19
78	1545	-16.91	-17.74	0.26	0.30 ± 0.54	0.87	1.41 ± 0.42
79	1192	-16.86	-18.14	1.27	...	0.94	1.85 ± 0.62
80	1857	-16.64	-17.32	0.90	...	0.53	0.73 ± 0.14
81	1075	-16.78	-17.55	0.63	0.87 ± 0.68	0.73	1.11 ± 0.47
82	1948	-16.06	-16.78	0.99	...	0.35	0.50 ± 0.09
83	1627	-16.46	-17.39	0.34	2.19 ± 0.34	0.59	1.03 ± 0.32
84	1440	-16.86	-17.66	0.88	1.21 ± 0.45	0.78	1.19 ± 0.44
85	230	-16.21	-16.96	0.96	1.41 ± 0.84	0.43	0.69 ± 0.29
86	2050	-16.36	-17.15	1.16	1.47 ± 0.52	0.47	0.29 ± 0.26
87	1993	-16.30	-17.02	0.95	1.03 ± 0.38	0.48	0.75 ± 0.27
88	751	-16.97	-17.92	1.72	2.05 ± 0.44	0.92	1.41 ± 0.51
89	1828	-16.78	-17.47	0.67	0.67 ± 0.55	0.72	1.26 ± 0.47
90	538	-16.24	-17.10	1.62	6.47 ± 0.86	0.44	0.63 ± 0.26
91	1407	-16.72	-17.43	0.17	0.23 ± 0.39	0.68	1.24 ± 0.42
92	1886	-16.25	-16.93	0.76	...	0.36	0.51 ± 0.10
93	1199	-15.47	-16.94	1.25	...	0.29	0.58 ± 0.16
94	1743	-16.33	-16.95	0.84	1.27 ± 0.75	0.45	0.40 ± 0.29
95	1539	-16.05	-17.12	0.25	0.26 ± 0.87	0.37	0.52 ± 0.11
96	1185	-16.77	-17.37	0.10	0.10 ± 0.79	0.78	0.89 ± 0.51
97	1826	-16.03	-16.71	0.98	1.11 ± 0.61	0.35	0.61 ± 0.22
98	1512	-16.25	-16.54	0.38	1.50 ± 0.42	0.43	0.61 ± 0.12
99	1489	-15.61	-16.41	0.45	...	0.22	0.32 ± 0.06
100	1661	-15.81	-17.40	0.70	1.26 ± 1.20	0.29	0.43 ± 0.08

¹ Running number, sorted by increasing B_T magnitude² Number in Virgo Cluster Catalog³ Absolute V magnitude⁴ Absolute z magnitude⁵ Projected distance from M87 (VCC 1316), in Mpc⁶ 3-dimensional distance from M87 (VCC 1316), in Mpc, using polynomial calibration from Paper XIII⁷ Stellar z luminosity ($10^9 L_\odot$)⁸ Stellar mass ($10^9 M_\odot$)

TABLE 2
GC FORMATION EFFICIENCIES IN ACS VIRGO CLUSTER SURVEY GALAXIES

No. (1)	VCC (2)	N_{GC} (3)	S_N (4)	$S_{N,z}$ (5)	T (6)	S_L (7)	S_M (8)	$S_{N,z,blue}$ (9)	$S_{N,z,red}$ (10)	T_{blue} (11)	T_{red} (12)	f_{red} (13)
1	1226	7813 ± 830	5.40 ± 0.57	2.20 ± 0.23	14.7 ± 3.4	1.23 ± 0.01	0.87 ± 0.18	1.57 ± 0.19	0.64 ± 0.14	10.4 ± 2.5	4.3 ± 1.3	0.29
2	1316	14660 ± 891	12.59 ± 0.77	4.19 ± 0.25	48.5 ± 13.0	2.33 ± 0.02	2.83 ± 0.74	3.04 ± 0.21	1.14 ± 0.15	35.2 ± 9.5	13.2 ± 3.9	0.27
3	1978	4745 ± 1099	5.16 ± 1.20	2.03 ± 0.47	14.0 ± 3.8	1.15 ± 0.02	0.84 ± 0.12	1.28 ± 0.38	0.75 ± 0.27	8.8 ± 2.9	5.2 ± 2.0	0.37
4	881	2660 ± 129	2.57 ± 0.12	1.03 ± 0.05	9.2 ± 1.9	0.56 ± 0.01	0.49 ± 0.10	0.87 ± 0.04	0.16 ± 0.03	7.7 ± 1.6	1.5 ± 0.4	0.16
5	798	1110 ± 181	1.29 ± 0.21	0.56 ± 0.09	6.0 ± 1.7	0.20 ± 0.01	0.21 ± 0.05	0.33 ± 0.07	0.23 ± 0.05	3.5 ± 1.1	2.4 ± 0.8	0.41
6	763	4301 ± 1201	5.20 ± 1.45	2.26 ± 0.63	18.2 ± 6.9	1.11 ± 0.03	0.89 ± 0.23	2.01 ± 0.51	0.24 ± 0.37	16.2 ± 5.9	2.0 ± 3.0	0.11
7	731	3246 ± 598	3.86 ± 0.71	1.45 ± 0.27	14.3 ± 4.2	0.85 ± 0.02	0.86 ± 0.20	0.80 ± 0.22	0.65 ± 0.16	7.9 ± 2.8	6.5 ± 2.2	0.45
8	1535	388 ± 117	1.09 ± 0.33	0.42 ± 0.13	5.0 ± 1.8	0.20 ± 0.00	0.25 ± 0.05	0.26 ± 0.10	0.16 ± 0.07	3.1 ± 1.4	1.9 ± 1.0	0.38
9	1903	803 ± 355	2.70 ± 1.19	1.07 ± 0.47	9.6 ± 4.8	0.68 ± 0.01	0.61 ± 0.14	0.55 ± 0.38	0.52 ± 0.27	4.9 ± 3.6	4.7 ± 2.7	0.49
10	1632	984 ± 198	2.82 ± 0.57	1.15 ± 0.23	10.3 ± 2.8	0.65 ± 0.01	0.61 ± 0.11	0.69 ± 0.19	0.46 ± 0.14	6.2 ± 2.0	4.1 ± 1.4	0.40
11	1231	376 ± 97	1.98 ± 0.51	0.88 ± 0.23	7.0 ± 2.4	0.32 ± 0.01	0.28 ± 0.06	0.50 ± 0.18	0.38 ± 0.13	4.0 ± 1.7	3.0 ± 1.3	0.43
12	2095	211 ± 34	1.03 ± 0.17	0.88 ± 0.14	4.0 ± 1.0	0.16 ± 0.00	0.14 ± 0.03	0.52 ± 0.11	0.35 ± 0.08	2.4 ± 0.7	1.6 ± 0.5	0.40
13	1154	218 ± 28	1.00 ± 0.13	0.42 ± 0.05	2.8 ± 0.6	0.12 ± 0.00	0.09 ± 0.02	0.22 ± 0.04	0.20 ± 0.03	1.5 ± 0.4	1.3 ± 0.3	0.48
14	1062	178 ± 30	1.06 ± 0.18	0.52 ± 0.09	3.4 ± 0.8	0.21 ± 0.00	0.16 ± 0.03	0.52 ± 0.07	0.00 ± 0.05	3.4 ± 0.7	0.0 ± 0.3	0.00
15	2092	103 ± 17	0.68 ± 0.11	0.23 ± 0.04	2.2 ± 0.5	0.08 ± 0.00	0.07 ± 0.01	0.13 ± 0.03	0.09 ± 0.02	1.3 ± 0.4	0.9 ± 0.3	0.39
16	369	179 ± 17	1.51 ± 0.14	1.23 ± 0.12	5.5 ± 1.4	0.28 ± 0.01	0.25 ± 0.06	0.58 ± 0.09	0.65 ± 0.08	2.6 ± 0.7	2.9 ± 0.8	0.53
17	759	200 ± 41	1.34 ± 0.27	0.54 ± 0.11	4.4 ± 1.3	0.24 ± 0.00	0.20 ± 0.05	0.35 ± 0.09	0.19 ± 0.07	2.9 ± 1.0	1.6 ± 0.6	0.35
18	1692	139 ± 23	1.09 ± 0.18	0.53 ± 0.09	4.1 ± 1.0	0.16 ± 0.01	0.16 ± 0.03	0.34 ± 0.07	0.19 ± 0.05	2.6 ± 0.7	1.5 ± 0.5	0.36
+19	1030	345 ± 80	2.27 ± 0.53	0.97 ± 0.22	25.9 ± 18.6	0.40 ± 0.01	1.06 ± 0.72	0.73 ± 0.18	0.24 ± 0.13	19.5 ± 14.1	6.4 ± 5.6	0.25
20	2000	205 ± 28	2.97 ± 0.41	1.12 ± 0.15	8.6 ± 1.9	0.53 ± 0.01	0.37 ± 0.06	0.97 ± 0.13	0.15 ± 0.08	7.5 ± 1.6	1.2 ± 0.7	0.13
21	685	196 ± 60	1.78 ± 0.54	0.75 ± 0.23	6.3 ± 2.3	0.40 ± 0.01	0.36 ± 0.08	0.54 ± 0.19	0.22 ± 0.13	4.5 ± 1.8	1.8 ± 1.2	0.29
22	1664	213 ± 31	2.35 ± 0.34	0.87 ± 0.13	8.2 ± 2.3	0.42 ± 0.01	0.37 ± 0.09	0.54 ± 0.10	0.33 ± 0.07	5.1 ± 1.5	3.1 ± 1.0	0.38
23	654	45 ± 16	0.50 ± 0.18	0.26 ± 0.09	2.0 ± 0.8	0.05 ± 0.00	0.05 ± 0.01	0.23 ± 0.08	0.04 ± 0.05	1.7 ± 0.7	0.3 ± 0.4	0.15
24	944	72 ± 10	0.87 ± 0.12	0.39 ± 0.05	2.5 ± 0.5	0.11 ± 0.01	0.08 ± 0.01	0.25 ± 0.04	0.14 ± 0.03	1.6 ± 0.4	0.9 ± 0.3	0.36
+25	1938	59.8 ± 9.2	0.64 ± 0.10	0.27 ± 0.04	2.4 ± 0.6	0.12 ± 0.01	0.11 ± 0.02	0.22 ± 0.04	0.05 ± 0.02	1.9 ± 0.5	0.5 ± 0.2	0.19
+26	1279	58 ± 11	0.72 ± 0.15	0.30 ± 0.06	2.7 ± 0.7	0.13 ± 0.01	0.11 ± 0.02	0.21 ± 0.05	0.09 ± 0.04	1.8 ± 0.6	0.8 ± 0.3	0.30
27	1720	62 ± 13	0.87 ± 0.18	0.33 ± 0.07	3.1 ± 1.0	0.12 ± 0.00	0.10 ± 0.03	0.22 ± 0.06	0.12 ± 0.04	2.0 ± 0.7	1.1 ± 0.5	0.36
28	355	100 ± 31	1.70 ± 0.53	0.69 ± 0.21	6.3 ± 2.4	0.11 ± 0.02	0.11 ± 0.03	0.53 ± 0.17	0.16 ± 0.12	4.9 ± 2.0	1.4 ± 1.2	0.23
29	1619	84 ± 19	1.52 ± 0.34	0.70 ± 0.16	4.9 ± 1.4	0.14 ± 0.01	0.10 ± 0.02	0.52 ± 0.13	0.19 ± 0.09	3.6 ± 1.1	1.3 ± 0.7	0.27
30	1883	83 ± 25	1.11 ± 0.34	0.42 ± 0.13	5.0 ± 1.9	0.16 ± 0.00	0.16 ± 0.04	0.29 ± 0.10	0.13 ± 0.07	3.4 ± 1.5	1.6 ± 0.9	0.31
31	1242	116 ± 24	2.05 ± 0.42	0.88 ± 0.18	7.6 ± 2.2	0.31 ± 0.01	0.26 ± 0.05	0.57 ± 0.15	0.31 ± 0.11	4.9 ± 1.6	2.7 ± 1.1	0.35
32	784	50 ± 14	0.95 ± 0.27	0.39 ± 0.11	3.0 ± 1.0	0.07 ± 0.01	0.05 ± 0.01	0.23 ± 0.09	0.17 ± 0.07	1.7 ± 0.7	1.3 ± 0.6	0.44
33	1537	31.4 ± 7.2	0.80 ± 0.18	0.33 ± 0.08	3.1 ± 1.0	0.00 ± 0.00	0.00 ± 0.00	0.29 ± 0.07	0.04 ± 0.03	2.7 ± 0.9	0.4 ± 0.3	0.12
34	778	74 ± 32	1.11 ± 0.48	0.72 ± 0.31	4.1 ± 2.0	0.14 ± 0.01	0.12 ± 0.03	0.51 ± 0.25	0.21 ± 0.18	2.9 ± 1.6	1.2 ± 1.1	0.29
35	1321	31.0 ± 9.0	0.94 ± 0.27	0.33 ± 0.10	4.4 ± 1.7	0.09 ± 0.01	0.08 ± 0.02	0.24 ± 0.08	0.09 ± 0.05	3.3 ± 1.3	1.2 ± 0.8	0.27
36	828	69.5 ± 9.8	1.52 ± 0.21	0.65 ± 0.09	5.1 ± 1.3	0.00 ± 0.00	0.00 ± 0.00	0.50 ± 0.08	0.15 ± 0.05	3.9 ± 1.1	1.2 ± 0.4	0.23
+37	1250	20.1 ± 7.3	0.52 ± 0.19	0.18 ± 0.07	5.5 ± 3.6	0.06 ± 0.01	0.14 ± 0.08	0.17 ± 0.06	0.01 ± 0.03	5.0 ± 3.3	0.4 ± 1.0	0.06
38	1630	47 ± 11	1.11 ± 0.26	0.44 ± 0.10	4.0 ± 1.3	0.12 ± 0.02	0.11 ± 0.03	0.26 ± 0.08	0.18 ± 0.06	2.4 ± 0.9	1.7 ± 0.7	0.41
39	1146	72 ± 12	1.93 ± 0.32	1.00 ± 0.17	8.3 ± 2.5	0.39 ± 0.02	0.40 ± 0.10	0.30 ± 0.12	0.70 ± 0.12	2.5 ± 1.1	5.8 ± 1.8	0.70
40	1025	141 ± 34	2.08 ± 0.50	0.84 ± 0.20	6.6 ± 2.1	0.25 ± 0.07	0.19 ± 0.08	0.75 ± 0.17	0.09 ± 0.11	5.9 ± 1.8	0.7 ± 0.9	0.11
41	1303	72 ± 18	2.10 ± 0.53	0.87 ± 0.22	6.9 ± 2.3	0.24 ± 0.03	0.18 ± 0.05	0.82 ± 0.18	0.05 ± 0.11	6.5 ± 2.1	0.4 ± 0.9	0.06
42	1913	71 ± 14	2.02 ± 0.40	0.90 ± 0.18	6.6 ± 2.1	0.31 ± 0.01	0.23 ± 0.06	0.74 ± 0.15	0.16 ± 0.09	5.4 ± 1.8	1.2 ± 0.8	0.18
+43	1327	11 ± 12	0.26 ± 0.29	0.14 ± 0.15	0.7 ± 0.7	0.07 ± 0.00	0.05 ± 0.01	0.09 ± 0.12	0.05 ± 0.09	0.4 ± 0.6	0.2 ± 0.4	0.36
44	1125	52.3 ± 8.5	1.23 ± 0.20	0.88 ± 0.14	6.5 ± 2.9	0.16 ± 0.01	0.20 ± 0.08	0.81 ± 0.13	0.07 ± 0.06	6.0 ± 2.7	0.5 ± 0.5	0.08
45	1475	81 ± 10	3.05 ± 0.40	1.38 ± 0.18	10.5 ± 2.5	0.33 ± 0.03	0.23 ± 0.05	1.33 ± 0.17	0.06 ± 0.06	10.1 ± 2.4	0.4 ± 0.5	0.04
+46	1178	25.3 ± 9.2	1.16 ± 0.42	0.46 ± 0.17	3.6 ± 1.5	0.12 ± 0.01	0.09 ± 0.02	0.31 ± 0.14	0.15 ± 0.10	2.4 ± 1.2	1.2 ± 0.8	0.33
47	1283	58.6 ± 9.3	2.02 ± 0.32	0.77 ± 0.12	6.5 ± 1.6	0.22 ± 0.03	0.16 ± 0.04	0.59 ± 0.10	0.18 ± 0.06	5.0 ± 1.3	1.5 ± 0.6	0.23
48	1261	35.1 ± 7.6	1.51 ± 0.33	0.72 ± 0.16	7.2 ± 2.9	0.29 ± 0.02	0.28 ± 0.10	0.60 ± 0.14	0.12 ± 0.08	6.0 ± 2.5	1.2 ± 0.9	0.17
49	698	114 ± 12	3.53 ± 0.38	1.50 ± 0.16	12.0 ± 3.5	0.56 ± 0.01	0.41 ± 0.11	1.23 ± 0.14	0.27 ± 0.07	9.8 ± 2.9	2.2 ± 0.8	0.18
50	1422	24.9 ± 6.0	1.62 ± 0.39	0.80 ± 0.19	6.5 ± 2.8	0.21 ± 0.02	0.17 ± 0.06	0.54 ± 0.16	0.26 ± 0.11	4.4 ± 2.0	2.1 ± 1.2	0.32
51	2048	17.2 ± 5.4	1.25 ± 0.39	0.64 ± 0.20	5.9 ± 2.8	0.19 ± 0.02	0.19 ± 0.07	0.49 ± 0.17	0.15 ± 0.11	4.5 ± 2.3	1.3 ± 1.1	0.23
52	1871	10.4 ± 5.0	1.24 ± 0.60	0.49 ± 0.24	4.6 ± 2.5	0.21 ± 0.07	0.17 ± 0.07	0.48 ± 0.21	0.01 ± 0.11	4.5 ± 2.3	0.1 ± 1.0	0.02
53	9	25.7 ± 6.4	1.57 ± 0.39	0.78 ± 0.19	8.3 ± 2.6	0.21 ± 0.02	0.20 ± 0.05	0.68 ± 0.17	0.09 ± 0.09	7.3 ± 2.4	1.0 ± 1.0	0.12
54	575	18.0 ± 6.1	0.77 ± 0.26	0.33 ± 0.11	3.6 ± 1.7	0.00 ± 0.06	-0.00 ± 0.06	0.26 ± 0.10	0.07 ± 0.06	2.8 ± 1.4	0.8 ± 0.7	0.21
55	1910	48.7 ± 8.4	5.38 ± 0.93	2.27 ± 0.39	23.2 ± 9.8	1.09 ± 0.04	1.12 ± 0.43	1.47 ± 0.32	0.79 ± 0.23	15.1 ± 6.7	8.1 ± 3.9	0.35
56	1049	8.4 ± 4.5	1.77 ± 0.95	0.97 ± 0.52	16.2 ± 15.1	0.05 ± 0.03	0.09 ± 0.08	0.75 ± 0.44	0.22 ± 0.28	12.4 ± 12.0	3.7 ± 5.5	0.23
57	856	43.4 ± 7.9	4.07 ± 0.74	2.17 ± 0.39	19.5 ± 8.3	0.55 ± 0.03	0.56 ± 0.22	1.80 ± 0.35	0.37 ± 0.19	16.2 ± 6.9	3.3 ± 2.1	0.17
58	140	21.3 ± 6.1	2.10 ± 0.60	1.05 ± 0.30	9.2 ± 3.8	0.18 ± 0.03	0.16 ± 0.06	0.79 ± 0.25	0.26 ± 0.16	6.9 ± 3.1	2.3 ± 1.6	0.25
59	1355	10.8 ± 5.6	1.07 ± 0.56	0.59 ± 0.30	5.9 ± 3.3	0.05 ± 0.01	0.07 ± 0.02	0.53 ± 0.26	0.06 ± 0.15	5.3 ± 2.8	0.6 ± 1.6	0.10
60	1087	66.0 ± 9.5	5.07 ± 0.73	2.31 ± 0.33	20.0 ± 7.1	0.87 ± 0.03	0.73 ± 0.24	2.17 ± 0.31	0.14 ± 0.12	18.8 ± 6.7	1.2 ± 1.1	0.06
+61	1297	4 ± 11	0.42 ± 1.00	0.16 ± 0.37	1.2 ± 3.0	0.15 ± 0.02	0.12 ± 0.02	0.11 ± 0.30	0.05 ± 0.22	0.9 ± 2.4	0.4 ± 1.7	0.31
62	1861	37.6 ± 7.4	3.44 ± 0.68	1.73 ± 0.34	13.0 ± 5.2	0.69 ± 0.07	0.49 ± 0.18	1.26 ± 0.29	0.47 ± 0.18	9.5 ± 3.9	3.5 ± 1.8	0.27
63	543	18.1 ± 5.5	1.97 ± 0.60	0.96 ± 0.29	8.3 ± 3.5	0.15 ± 0.03	0.14 ± 0.05	0.96 ± 0.27	0.00 ± 0.11	8.3 ± 3.4	0.0 ± 0.9	0.00
64	1431	60.6 ± 9.3	6.72 ± 1.03	3.03 ± 0.46	27.5 ± 10.2	0.78 ± 0.04	0.70 ± 0.24	2.57 ± 0.41	0.45 ± 0.21	23.4 ± 8.7	4.1 ± 2.4	0.15
65	1528	40.7 ± 7.6	5.57 ± 1.04	2.46 ± 0.46	24.9 ± 8.7	0.66 ± 0.04	0.69 ± 0.21	2.24 ± 0.42	0.22 ± 0.19	22.7 ± 7.9	2.2 ± 2.0	0.09
66	1695	14.4 ± 5.7	1.45 ± 0.58	0.68 ± 0.27	8.5 ± 5.2	0.09 ± 0.03	0.10 ± 0.06	0.48 ± 0.22	0.20 ± 0.15	6.0 ± 3.9	2.5 ± 2.2	0.29
67	1833	18.1 ± 5.5	2.55 ± 0.77	1.26 ± 0.38	21.1 ± 13.5	0.15 ± 0.04	0.25 ± 0.16	0.87 ± 0.32	0.39 ± 0.22	14.6 ± 9.8	6.5 ± 5.2	0.31
68	437	42.1 ± 7.9	3.13 ± 0.59	1.40 ± 0.26	15.0 ± 7.2	0.46 ± 0.04	0.34 ± 0.15	1.32 ± 0.24	0.08 ± 0.10	14.1 ± 6.8	0.9 ± 1.2	0.06
69	2019	23.9 ± 6.1	2.72 ± 0.69	1.28 ± 0.33	23.5 ± 17.8	0.72 ± 0.05	1.19 ± 0.85	1.28 ± 0.31	0.00 ± 0.11	23.5 ± 17.6	0.0 ± 2.1	0.00
70	33	2.2 ± 4.2	0.61 ± 1.17	0.34 ± 0.66	5.1 ± 10.1	-0.13 ± 0.07	-0.21 ± 0.16	0.22 ± 0.53	0.12 ± 0.38	3.3 ± 8.1	1.8 ±	

TABLE 2 — *Continued*

No. (1)	VCC (2)	N_{GC} (3)	S_N (4)	$S_{N,z}$ (5)	T (6)	S_L (7)	S_M (8)	$S_{N,z,blue}$ (9)	$S_{N,z,red}$ (10)	T_{blue} (11)	T_{red} (12)	f_{red} (13)
78	1545	54.2 ± 8.8	9.37 ± 1.52	4.34 ± 0.71	38.5 ± 13.0	1.02 ± 0.07	0.76 ± 0.23	3.91 ± 0.64	0.43 ± 0.29	34.6 ± 11.8	3.8 ± 2.8	0.10
†79	1192	-6 ± 13	-1.12 ± 2.42	-0.34 ± 0.74	-3.4 ± 7.3	-0.39 ± 0.05	-0.31 ± 0.11	-0.21 ± 0.61	-0.13 ± 0.45	-2.1 ± 5.9	-1.3 ± 4.4	0.00
80	1857	10.8 ± 5.9	2.39 ± 1.31	1.28 ± 0.70	14.8 ± 8.6	0.32 ± 0.09	0.29 ± 0.12	0.78 ± 0.56	0.50 ± 0.42	9.1 ± 6.7	5.8 ± 5.0	0.39
1075	16.5 ± 5.2	3.19 ± 1.01	1.58 ± 0.50	14.8 ± 7.8	0.33 ± 0.06	0.31 ± 0.14	1.58 ± 0.46	0.00 ± 0.18	14.8 ± 7.6	0.0 ± 1.7	0.00	
82	1948	2.5 ± 3.0	0.94 ± 1.13	0.48 ± 0.58	5.0 ± 6.1	-0.28 ± 0.17	-0.22 ± 0.12	0.48 ± 0.50	0.00 ± 0.29	5.0 ± 5.3	0.0 ± 3.0	0.00
83	1627	3.6 ± 3.7	0.94 ± 0.97	0.40 ± 0.41	3.5 ± 3.8	1.21 ± 0.13	1.05 ± 0.34	0.40 ± 0.36	0.00 ± 0.21	3.5 ± 3.3	0.0 ± 1.8	0.00
84	1440	26.7 ± 6.8	4.81 ± 1.22	2.30 ± 0.58	22.5 ± 10.1	0.29 ± 0.05	0.31 ± 0.12	1.93 ± 0.51	0.37 ± 0.28	18.9 ± 8.6	3.6 ± 3.1	0.16
85	230	28.7 ± 6.7	9.39 ± 2.19	4.73 ± 1.10	41.4 ± 20.0	5.45 ± 1.17	3.68 ± 1.73	4.64 ± 1.03	0.09 ± 0.41	40.5 ± 19.4	0.8 ± 3.6	0.02
86	2050	9.2 ± 4.3	2.63 ± 1.23	1.27 ± 0.60	31.5 ± 32.0	0.21 ± 0.06	0.43 ± 0.41	1.27 ± 0.54	0.00 ± 0.25	31.5 ± 31.4	0.0 ± 6.1	0.00
87	1993	-1.6 ± 2.1	-0.48 ± 0.63	-0.25 ± 0.33	-2.1 ± 2.9	-0.07 ± 0.08	0.29 ± 0.13	-0.03 ± 0.30	-0.22 ± 0.29	-0.3 ± 2.6	-1.9 ± 2.6	0.00
88	751	9.2 ± 4.3	1.49 ± 0.70	0.62 ± 0.29	6.5 ± 3.9	0.13 ± 0.04	0.11 ± 0.06	0.62 ± 0.27	0.00 ± 0.12	6.5 ± 3.6	0.0 ± 1.3	0.00
89	1828	20.4 ± 5.8	3.94 ± 1.12	2.10 ± 0.60	16.3 ± 7.7	0.95 ± 0.08	0.78 ± 0.30	2.10 ± 0.56	0.00 ± 0.22	16.3 ± 7.5	0.0 ± 1.7	0.00
90	538	0.6 ± 3.5	0.19 ± 1.11	0.09 ± 0.51	0.9 ± 5.5	-0.31 ± 0.22	-0.25 ± 0.19	0.09 ± 0.42	0.00 ± 0.29	0.9 ± 4.6	0.0 ± 3.1	0.00
91	1407	49.7 ± 8.6	10.18 ± 1.76	5.30 ± 0.92	40.2 ± 15.5	0.69 ± 0.07	0.50 ± 0.18	4.61 ± 0.82	0.69 ± 0.41	35.0 ± 13.5	5.2 ± 3.6	0.13
92	1886	3.9 ± 2.6	1.24 ± 0.82	0.66 ± 0.44	7.7 ± 5.3	0.29 ± 0.06	0.41 ± 0.11	0.66 ± 0.41	0.00 ± 0.17	7.7 ± 5.0	0.0 ± 1.9	0.00
†93	1199	-9 ± 14	-6.24 ± 9.23	-1.60 ± 2.37	-16.6 ± 24.9	-3.39 ± 0.24	-2.55 ± 0.74	-0.90 ± 1.93	-0.70 ± 1.45	-9.3 ± 20.1	-7.3 ± 15.2	0.00
94	1743	9.8 ± 6.4	2.88 ± 1.88	1.63 ± 1.06	24.6 ± 23.9	-0.03 ± 0.29	-0.13 ± 0.55	1.11 ± 0.87	0.52 ± 0.62	16.7 ± 17.8	7.9 ± 10.9	0.32
95	1539	31.0 ± 7.0	11.83 ± 2.67	4.40 ± 0.99	59.4 ± 18.7	2.41 ± 0.33	1.73 ± 0.40	4.40 ± 0.93	0.00 ± 0.35	59.4 ± 18.1	0.0 ± 4.7	0.00
†96	1185	14.0 ± 5.7	2.73 ± 1.11	1.58 ± 0.64	15.7 ± 11.0	0.20 ± 0.04	0.26 ± 0.16	1.45 ± 0.56	0.13 ± 0.31	14.4 ± 9.9	1.3 ± 3.1	0.08
97	1826	4.5 ± 3.9	1.74 ± 1.51	0.93 ± 0.81	7.3 ± 6.9	0.08 ± 0.11	-0.01 ± 0.12	0.93 ± 0.71	0.00 ± 0.40	7.3 ± 6.1	0.0 ± 3.1	0.00
98	1512	4.7 ± 3.8	1.48 ± 1.20	1.14 ± 0.92	7.7 ± 6.5	-0.40 ± 0.58	-0.42 ± 0.42	1.14 ± 0.81	0.00 ± 0.44	7.7 ± 5.7	0.0 ± 3.0	0.00
99	1489	11.7 ± 4.8	6.69 ± 2.74	3.19 ± 1.31	36.9 ± 16.7	0.46 ± 0.16	0.34 ± 0.14	2.20 ± 1.08	0.99 ± 0.75	25.4 ± 13.3	11.4 ± 8.9	0.31
100	1661	10.2 ± 4.7	4.83 ± 2.23	1.12 ± 0.51	23.9 ± 12.0	0.08 ± 0.08	0.06 ± 0.14	1.12 ± 0.46	0.00 ± 0.22	23.9 ± 11.0	0.0 ± 4.7	0.00

1 Running number, sorted by increasing B_T magnitude

2 Number in Virgo Cluster Catalog

3 Total number of globular clusters

4 Specific frequency

5 Specific frequency in z bandpass

6 N_{GC} normalized to stellar mass of $10^9 M_\odot$

7 Percentage of galaxy z luminosity in GCs

8 Percentage of galaxy stellar mass in GCs

9 Specific frequency in z for blue GCs

10 Specific frequency in z for red GCs

11 T for blue GCs

12 T for red GCs

13 Fraction of red GCs

† Quantities calculated using an $R=70''$ aperture around galaxy

‡ Quantities possibly affected by nearby dE VCC 1941, which has been masked

* Mass-to-light ratio (i.e. optical-IR colors) suspect.